

Journal Pre-proof



mRNA vaccination of naive and COVID-19-recovered individuals elicits potent memory B cells that recognize SARS-CoV-2 variants

Aurélien Sokal, Giovanna Barba-Spaeth, Ignacio Fernández, Matteo Broketa, Imane Azzaoui, Andrea de La Selle, Alexis Vandenberghe, Slim Fourati, Anais Roeser, Annalisa Meola, Magali Bouvier-Alias, Etienne Crickx, Laetitia Languille, Marc Michel, Bertrand Godeau, Sébastien Gallien, Giovanna Melica, Yann Nguyen, Virginie Zarrouk, Florence Canoui-Poitrine, France Noizat-Pirenne, Jérôme Megret, Jean-Michel Pawlotsky, Simon Fillatreau, Pierre Bruhns, Felix A. Rey, Jean-Claude Weill, Claude-Agnès Reynaud, Pascal Chappert, Matthieu Mahévas

PII: S1074-7613(21)00396-4

DOI: <https://doi.org/10.1016/j.immuni.2021.09.011>

Reference: IMMUNI 4715

To appear in: *Immunity*

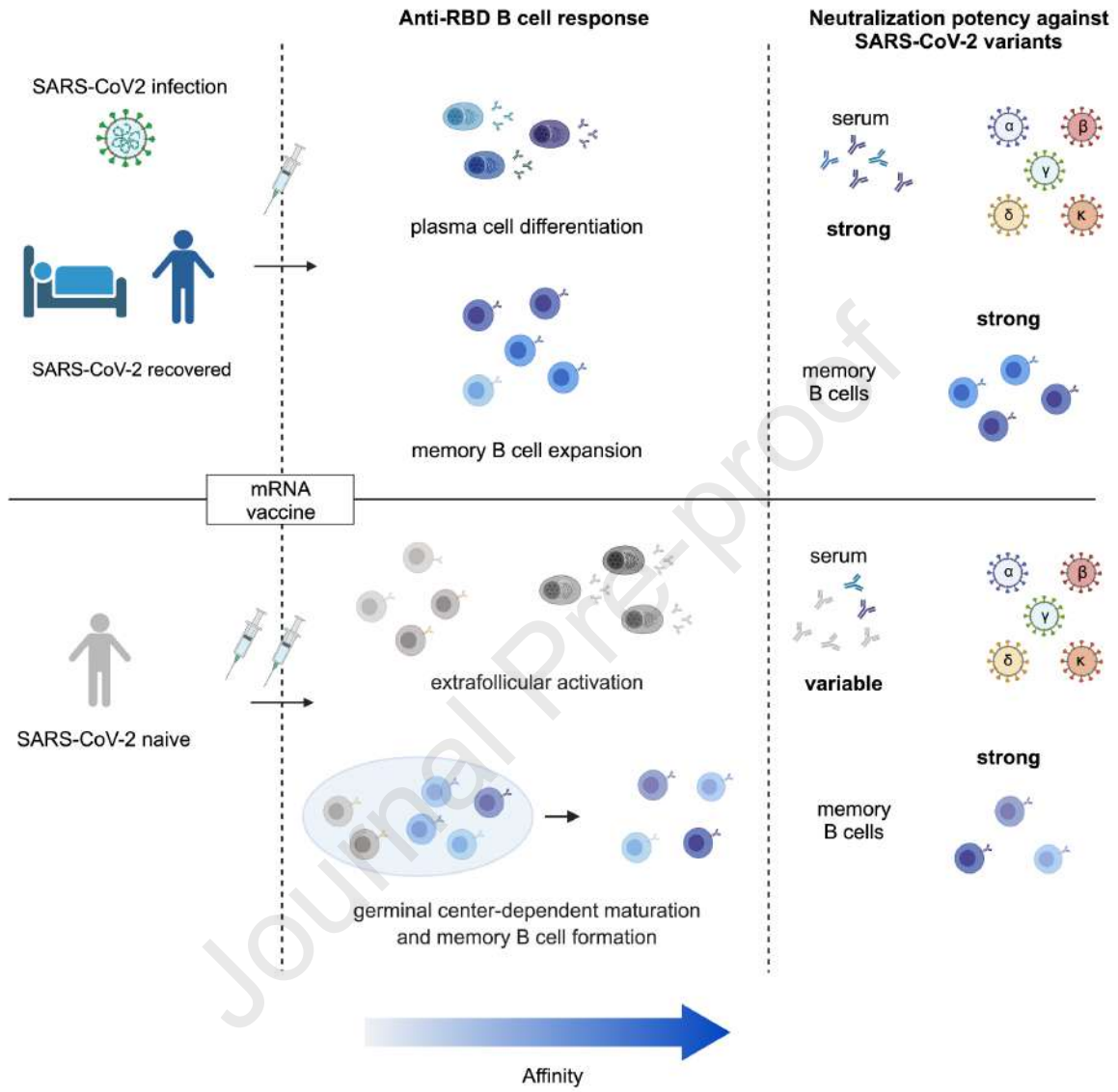
Received Date: 17 June 2021

Revised Date: 20 July 2021

Accepted Date: 14 September 2021

Please cite this article as: Sokal, A., Barba-Spaeth, G., Fernández, I., Broketa, M., Azzaoui, I., de La Selle, A., Vandenberghe, A., Fourati, S., Roeser, A., Meola, A., Bouvier-Alias, M., Crickx, E., Languille, L., Michel, M., Godeau, B., Gallien, S., Melica, G., Nguyen, Y., Zarrouk, V., Canoui-Poitrine, F., Noizat-Pirenne, F., Megret, J., Pawlotsky, J.-M., Fillatreau, S., Bruhns, P., Rey, F.A., Weill, J.-C., Reynaud, C.-A., Chappert, P., Mahévas, M., mRNA vaccination of naive and COVID-19-recovered individuals elicits potent memory B cells that recognize SARS-CoV-2 variants, *Immunity* (2021), doi: <https://doi.org/10.1016/j.immuni.2021.09.011>.

This is a PDF file of an article that has undergone enhancements after acceptance, such as the addition of a cover page and metadata, and formatting for readability, but it is not yet the definitive version of record. This version will undergo additional copyediting, typesetting and review before it is published in its final form, but we are providing this version to give early visibility of the article. Please note that, during the production process, errors may be discovered which could affect the content, and all legal disclaimers that apply to the journal pertain.



mRNA vaccination of naive and COVID-19-recovered individuals elicits potent memory B cells that recognize SARS-CoV-2 variants

Aurélien Sokal^{*1,2}, Giovanna Barba-Spaeth^{*3}, Ignacio Fernández^{*3}, Matteo Broketa^{*4}, Imane Azzaoui^{**2,5}, Andrea de La Selle^{**1,2}, Alexis Vandenberghe^{**2,5}, Slim Fourati^{**6,7}, Anais Roeser^{1,2}, Annalisa Meola³, Magali Bouvier-Alias^{6,7}, Etienne Crickx^{1,2}, Laetitia Languille², Marc Michel², Bertrand Godeau², Sébastien Gallien⁸, Giovanna Melica⁸, Yann Nguyen⁹, Virginie Zarrouk⁹, Florence Canoui-Poitrine¹⁰, France Noizat-Pirenne^{5,11}, Jérôme Megret¹², Jean-Michel Pawlotsky^{6,7}, Simon Fillatreau¹, Pierre Bruhns^{†4}, Felix A. Rey^{†3}, Jean-Claude Weill^{†1}, Claude-Agnès Reynaud^{†1}, Pascal Chappert^{†1,13} & Matthieu Mahévas^{†1,2,5}.

* these authors contributed equally.

** these authors contributed equally.

†shared senior authorship

1. Institut Necker Enfants Malades (INEM), INSERM U1151/CNRS UMS 8253, Université de Paris, Paris, France.

2. Service de Médecine Interne, Centre Hospitalier Universitaire Henri-Mondor, Assistance Publique-Hôpitaux de Paris (AP-HP), Université Paris-Est Créteil (UPEC), Créteil, France.

3. Institut Pasteur, Unité de Virologie Structurale, CNRS UMR 3569, Paris, France.

4. Institut Pasteur, Unité Anticorps en thérapie et pathologie, UMR 1222 INSERM, France.

5. INSERM U955, équipe 2. Institut Mondor de Recherche Biomédicale (IMRB), Université Paris-Est Créteil (UPEC), Créteil, France.

6. Département de Virologie, Bactériologie, Hygiène et Mycologie-Parasitologie, Centre Hospitalier Universitaire Henri-Mondor, Assistance Publique-Hôpitaux de Paris (AP-HP), Créteil, France.

7. INSERM U955, équipe 18. Institut Mondor de Recherche Biomédicale (IMRB), Université Paris-Est Créteil (UPEC), Créteil, France.

8. Service de Maladies Infectieuses, Centre Hospitalier Universitaire Henri-Mondor, Assistance Publique-Hôpitaux de Paris (AP-HP), Université Paris-Est Créteil (UPEC), Créteil, France.

9. Service de Médecine interne, Hôpital Beaujon, Assistance Publique-Hôpitaux de Paris, Université de Paris, Clichy, France.

10. Département de Santé Publique, Unité de Recherche Clinique (URC), CEpiA (Clinical Epidemiology and Ageing), EA 7376- Institut Mondor de Recherche Biomédicale (IMRB), Centre Hospitalier Universitaire Henri-Mondor, Assistance Publique-Hôpitaux de Paris (AP-HP), Université Paris-Est Créteil (UPEC), Créteil, France.

11. Etablissement Français du Sang (EFS) Ile de France, Créteil, France.
12. Plateforme de Cytométrie en Flux, Structure Fédérative de Recherche Necker, INSERM US24-CNRS UMS3633, Paris, France.
13. Inovarion, Paris, France.

To whom correspondence should be addressed: matthieu.mahevas@aphp.fr, pascal.chappert@inserm.fr, claire-agnes.reynaud@inserm.fr, jean-claude.weill@inserm.fr

Lead Contact: Matthieu Mahévas (matthieu.mahevas@aphp.fr).

Summary

In addition to serum immunoglobulins, memory B cell (MBC) generation against SARS-CoV-2 represents another layer of immune protection, but the quality of MBC responses in naive and COVID-19-recovered individuals after vaccination remains ill-defined. We studied longitudinal cohorts of naive individuals and disease-recovered patients for up to 2 months after SARS-CoV-2 mRNA vaccination. We assessed the quality of the memory response by analysis of VDJ repertoires, affinity and neutralization against variants of concern (VOCs), using unbiased cultures of 2452 MBCs. Upon boosting, the MBC pool of recovered patients selectively expanded, further matured and harbored potent neutralizers against VOCs. Although naïve individuals had weaker neutralizing serum responses, half of their RBD-specific MBCs displayed high affinity towards multiple VOCs, including delta (B.1.617.2), and one-third retained neutralizing potency against beta (B.1.351). Our data suggest that an additional challenge in naive vaccinees could recall such affinity-matured MBCs and allow them to respond efficiently to VOCs.

Introduction

The COVID-19 pandemic caused by severe acute respiratory syndrome coronavirus 2 (SARS-CoV-2) has resulted in more than 220 million infections and at least 4.5 million deaths, as of Sept 6, 2021. Vaccination represents the main hope to control the pandemic. COVID-19 vaccines containing nucleoside-modified mRNA encoding the original Wuhan-Hu-1 SARS-CoV-2 spike glycoprotein (S) developed by Pfizer/BioNTech (BNT162b2) and Moderna (mRNA-1273) are now being deployed worldwide. They were shown to be safe, highly effective to prevent infection and to control disease severity (Baden et al., 2021; Dagan et al., 2021; Polack et al., 2020).

The emergence of SARS-CoV-2 variants bearing mutations in key B cell epitopes, however, has raised concerns that viral evolution will erode natural immunity or the protection offered by vaccination. One early mutation in the spike protein (D614G), which shifts the equilibrium between the open and closed protein conformation without modifying antibody neutralization, has become globally dominant (Plante et al., 2021; Weissman et al., 2021; Yurkovetskiy et al., 2020). Since then, novel variants of concern (VOCs) or of interest (VOIs) have spread around the world, with additional combinations of mutations and deletions mainly located in the ACE-2 receptor-binding domain (RBD) and the N-terminal domain of the S protein. Mutations in the RBD are of particular importance, as a large fraction of neutralizing antibodies elicited after infection and vaccination target this domain. The selective advantage provided by these mutations has resulted in their increasing prevalence: N501Y in the B.1.1.7 (alpha) variant; K417N, E484K, N501Y in the B.1.351 (beta) variant, K417T, E484K, N501Y in the P.1 (gamma) variant and L452R, E484Q, or L452R, T478K in the B1.617.1 (kappa) and B1.617.2 (delta) variants, respectively (Cherian et al., 2021; Davies et al., 2021; Greaney et al., 2021a; Tegally et al., 2021).

Higher infectiousness of the B.1.1.7 variant does not impair neutralizing antibody response (Davies et al., 2021; Garcia-Beltran et al., 2021; Planas et al., 2021a; Supasa et al., 2021). By contrast, E484K and K417T/N mutations in the B.1.351 and P.1 strains markedly reduced the neutralization potency in COVID-19 recovered or naive vaccinated individuals (Cele et al., 2021; Edara et al., 2021; Greaney et al., 2021a; Hoffmann et al., 2021; Planas et al., 2021a; Wang et al., 2021a; Xie et al., 2021). Even though infection with VOCs or VOIs remain possible after successful vaccination (Hacisuleyman et al., 2021), the effectiveness of the BNT162b2 vaccine against B.1.351 in preventing severe disease was recently demonstrated during the vaccination campaign in Qatar (Abu-Raddad et al., 2021).

In parallel to the rapid antibody secreting cell (ASC) and serum immunoglobulin G (IgG) response, the progressive generation of memory B cells (MBCs) against the SARS-CoV-2 virus represents another layer of immune protection (Dugan et al., 2021; Gaebler et al., 2021; Rodda et al., 2021; Sakharkar et al., 2021; Sokal et al., 2021). MBCs not only persist after infection but continuously evolve and mature by progressive acquisition of somatic mutations in their variable region genes to improve affinity through an ongoing germinal center response, potentially driven by antigenic persistence (Gaebler et al., 2021, 2021; Rodda et al., 2021; Sokal et al., 2021). MBCs further drive the recall response after antigenic rechallenge by differentiating into new antibody-secreting cells (ASCs) displaying the diverse array of high-affinity-antibodies contained in the MBC repertoire. However, a strong convergence of the anti-RBD response across COVID-19 recovered and naive vaccinated individuals shaped by recurrent germline gene families has been described. This could favor viral mutational escape as one single mutation in the RBD can confer a selective advantage by reducing binding and neutralizing activity of antibodies (Garcia-Beltran et al., 2021; Greaney et al., 2021a).

Upon vaccination, COVID-19 recovered patients showed a striking expansion of RBD-specific MBCs (Goel et al., 2021; Wang et al., 2021b) and elicited a strong serum antibody response including cross-neutralizing antibodies against VOCs (Ebinger et al., 2021; Konstantinidis et al., 2021; Krammer et al., 2021; Manisty et al., 2021; Saadat et al., 2021; Samanovic et al., 2021; Stamatatos et al., 2021; Wang et al., 2021b). Much less is known about the long-term stability, dynamics and functionality of the MBC repertoire after repeated antigenic stimulation. How the MBC pool will contract or expand its diversity after a new challenge is of major importance in the context of vaccination schemes with repeated homologous or heterologous booster doses and coexistence of multiple VOCs.

Here, we longitudinally characterized the dynamics, clonal evolution, affinity and neutralization capacity of anti-SARS-CoV-2 MBCs after mRNA vaccination in naive and SARS-CoV-2 recovered individuals from the analysis of over two thousand naturally expressed antibodies from single-cell cultured RBD-specific MBCs. We demonstrate that mRNA vaccination selects high-affinity neutralizing clones without compromising the overall MBC pool.

Results

mRNA vaccination boosts serum IgG levels in SARS-CoV-2-recovered and naive individuals.

The B cell immune response elicited by vaccination was analyzed in two cohorts, one of patients previously infected with SARS-CoV-2 (SARS-CoV-2 recovered) and one of virus-naive individuals (SARS-CoV-2 naive). We previously characterized the longitudinal evolution and maturation, up to 6 months after infection, of SARS-CoV-2-responding B cells in a cohort of mild ambulatory (M-CoV) and severe forms of COVID-19 requiring oxygen (S-CoV) (Sokal et al., 2021). Thirty-four patients from this original cohort were included in this study along with 9 additional COVID-19 patients, for a total of 17 S-CoV and 26 M-CoV (**Figure 1A and Table S1A and S1B**). All patients in this first cohort received one dose of Pfizer-BioNTech mRNA (BNT162b2) vaccine between 6 and 12 months post infection (median 309 days post COVID-19 symptom onset, range: 183-362 days, **see Table S1C**). This unique vaccine dose for SARS-CoV-2 recovered patients was referred to as “boost”. As a parallel cohort, we recruited 25 healthcare workers with no clinical history of COVID-19 and no serological evidence of previous SARS-CoV-2 infection. SARS-CoV-2 naive individuals in this second cohort received 2 doses of BNT162b2 vaccine as part of the French vaccination campaign. The second vaccine dose, also referred to as “boost”, was received in median 28 days after the first dose of vaccine, referred to as “prime”. Post-boost blood samples were collected from all vaccinated participants in median 8 days (range 5-22 days) and 2 months after the injection (**Figure 1A and see Table S1C**). Eight SARS-CoV-2 naive donors were additionally sampled after initial priming.

We first measured the pre- and post-boost evolution of IgG serum titers against the WT RBD in both cohorts. Anti-RBD IgG titers remained stable between 6 (M6) and 12 months (M12) post-infection in SARS-CoV-2 recovered patients, with only a mild decrease seen in S-CoV patients (**Figure 1B**). In line with previous reports, a single dose of mRNA vaccine elicited a strong recall response in all patients, with anti-RBD IgG titers increasing on average by 24-fold in S-CoV and 53-fold in M-CoV patients as compared with pre-boost titers (**Figure 1C and S1A, Table S2A**). In SARS-CoV-2 naive individuals, the mRNA vaccine boost also induced a robust anti-RBD IgG response (average of 25-fold-increase) although titers remained inferior to SARS-CoV-2-recovered patients at all time points (mean 10,870 vs. 75,511 AU/mL in S-CoV and 55,024 in M-CoV, P -value 0.005 and <0.0001 ,

respectively). Despite contraction of the response in all groups, anti-RBD IgG were at least 10-fold higher than pre-boost/prime titers at 2 months post boost (**Figure 1C and S2A**).

Twelve months after infection, all sera from SARS-CoV-2 recovered patients demonstrated neutralization potential in a focus reduction assay against an authentic SARS-CoV-2 virus carrying the dominant D614G amino acid change in the S1 domain of its Spike protein (**Figure 1D-E and Figure S1B-C**). This potential was more pronounced in S-CoV than in M-CoV but, as expected, was similarly reduced in both groups against the B.1.351 VOC strain, harboring three mutations in its RBD (N501Y, which increases the affinity for the ACE2 receptor, E484K and K417N, which are implicated in escape from neutralizing antibodies (Harvey et al., 2021)), along with several mutations in other Spike domains. As previously reported (Goel et al., 2021; Reynolds et al., 2021; Stamatatos et al., 2021; Wang et al., 2021b), a boost mRNA vaccine strongly enhanced the overall neutralizing potency of SARS-CoV-2 recovered patients against both the D614G and the B.1.351 viruses, with all S-CoV and M-CoV sera achieving $IC_{50} > 1/2560$ for the D614G strain. All sera from S-CoV patients also reached strong neutralizing potency against the B.1.351 and B.1.617.2 (Delta) virus ($IC_{50} > 1/2560$), although we cannot exclude differences above the tested dilution range for both VOCs (**Figure 1D-E, Figure S1B, Table S2B**). For M-CoV patients, the gain in neutralization potency against B.1.351 and B.1.617.2 VOCs was also clear albeit more modest for the B.1.351 virus. Sera from all naive individuals also showed detectable neutralizing activity against the D614G strain at the final time point in our study (mean IC_{50} : 1/988, range ≥ 2560 to 1/103), although never reaching IC_{50} seen in SARS-CoV-2 recovered patients. This potency was further reduced against the B.1.351 VOC strain (mean IC_{50} 1/332), with 8 out of 23 patients (35%) displaying IC_{50} below 1/100 against this variant; in contrast, all naive patients tested displayed low, but detectable neutralization capacity against the B.1.617.2 variant.

Together these data show that a boost of mRNA vaccine based on the Wuhan-Hu-1 S protein induces a strong recall response in all SARS-CoV-2 recovered patients, with strong neutralizing IgG serum titers against both D614G SARS-CoV-2 as well as B.1.351 and B.1.617.2 VOCs in most individuals. The lower neutralization potency achieved in naive individuals suggests a key role for the matured MBC pool present in SARS-CoV2 recovered patients in modeling the quality of the vaccine response, including the cross-neutralization of VOCs.

mRNA vaccination mobilizes the memory B cells in SARS-CoV-2-recovered patients.

Similar to the serum IgG titers, the percentage of RBD-specific and S-specific CD27⁺IgD⁻ B cells remained stable between 6 and 12 months in SARS-CoV-2 recovered patients, irrespectively of initial disease severity, thus confirming the generation of germinal-center-derived long-lived MBCs after natural infection (**Figure 2A-B and Figure S2A-B**). RBD-specific MBCs, which represent a large fraction of the neutralizing MBC pool against SARS-CoV-2, substantially expanded after one dose of mRNA vaccine before a modest contraction at 2 months (**Figure 2C and Figure S2C, Table S2**). In contrast, only low numbers of RBD-specific B cells were detectable in naive individuals after prime with a non-significant impact of boost vaccination (**Figure 2C**), although RBD-specific ASCs were observed in all donors in the early steps of the post-boost response (**Figure S2D**). The frequency of RBD-specific MBCs persisting 2 months after the boost in naive individuals remained significantly lower than the frequency of MBCs observed in SARS-CoV-2 recovered patients before vaccination (**Figure 2C**), with similar profiles observed for spike-specific MBCs (**Figure S2E**). The overall frequency of spike-specific MBCs in naive individuals at two months after the boost (three months after the prime) appeared even reduced as compared to the three-month post-infection time point in SARS-CoV-2 recovered patients (**Figure S2F**).

Unsupervised analysis of CD19⁺IgD⁻ switched B cell populations, using a multi-parametric flow panel which we previously used to describe the initial response against SARS-CoV-2 in these patients (Sokal et al., 2021), showed that RBD-specific cells mostly resided in the CD21⁺CD27⁺IgD⁻CD38^{int/-}CD71^{int/-} resting MBC compartment before vaccination (**Figure 2D-F, Table S2C and D**). These cells rapidly switched to a CD27⁺CD38^{int/+}CD71⁺ activated B cell phenotype (ABC cluster), in the first 7 days after the boost, together with the emergence of a population of RBD⁺ CD38^{high}CD27^{high} ASCs. The persistent expression of the BCR on the surface of these cells harboring a classical ASC phenotype suggests that they were mainly newly generated plasmablasts. These activated subsets progressively contracted and matured as resting MBCs at the latest time point in our study. Atypical MBCs (DN2; IgD⁻CD27^{+/-}CD11c⁺) and ASC precursors (DN1; IgD⁻CD27⁻) RBD-specific clusters were also observed, with a small DN2 fraction persisting up to two months post boost, notably in S-CoV patients (**Figure 2F**).

The low numbers of RBD-specific B cells in naive patients precluded a robust unsupervised analysis, and we therefore characterized the phenotype of RBD-specific MBCs

from the whole cohort using manual gating, based on the CD19 and CD71 expression profiles, to delineate activated B cells ($CD19^{high}CD71^{+}$) and resting MBCs ($CD19^{+}CD71^{low}$) among RBD-specific cells over time. A large fraction of RBD-specific MBCs acquired a $CD19^{high}CD71^{+}$ activated B cell phenotype in the days following the boost in naive individuals, similarly to M-CoV and S-CoV patients (**Figure 2G-H, Table S2E**), demonstrating that vaccine induced a robust expansion of an RBD-specific activated B cell population in all groups of donors.

The proportion of RBD-specific activated B cells decreased over time, favoring an increase of RBD-specific resting MBCs consistent with the contraction of the vaccine response. This contraction appeared more pronounced in SARS-CoV-2 recovered patients, suggesting the persistence of a GC output in naive individuals (**Figure 2H**). Similar kinetics were observed for S-specific B cells (**Figure S2G**), although it should be noted that RBD-specific B cells still represented a smaller proportion of S-specific cells in naive than in SARS-CoV-2 recovered individuals at the two-month time point (**Figure 2I and S2H**).

mRNA vaccination maintains the overall diversity of the memory B cell repertoire.

To address how mRNA vaccine boost affects the MBC repertoire, we then performed single cell sorting and culture of RBD-specific MBCs before, 7 days and 2 months after the boost in SARS-CoV-2 recovered patients, and 2 months after the boost in naive individuals (**Figure 3A**). We obtained a total of 2452 V_H sequences from 4 S-CoV, 4-M-CoV and 3 naive individuals (**Table S1A and C, Table S3A-H3**). Clonally expanded RBD-specific MBC were found before vaccination in all SARS-CoV-2 recovered patients, representing 13-34% of total V_H sequences for each donor (**Figure 3B and Figure S3A**). Vaccine-activated MBC showed no evidence of further clonal dominance and conserved their overall diversity, despite the major increase in MBC numbers. The fraction of the repertoire belonging to these clones varies from 19-39%, and remains comparable during contraction, with clones persisting over the pre/post vaccination period observed in all SARS-CoV-2 recovered patients. This overall clonal stability was reflected by similar Shannon entropy values at all studied time points (**Figure S3B**). Similar clonal expansion was observed in naive individuals (**Figure 3C**), which also harbored high frequency of convergent RBD-specific clones with SARS-CoV-2 recovered patients based on V-D-J sequences (**Figure 3D**).

We previously reported a progressive accumulation of somatic mutations in RBD-specific clones up to 6 months after infection in this cohort of SARS-CoV-2 recovered patients (Sokal et al., 2021). The number of mutations in RBD-specific V_H sequences

remained stable between 6 and 12 months. In contrast, V_H mutation numbers were increased shortly after the boost and maintained in the MBC pool 2 months after (**Figure 3E**). This evolution in mutation profile could further be confirmed at the individual level for 2 patients with complete follow-up from 3 or 6 months post symptom onset to 2 months after boost (**Figure S3C-D, Table S3A**). This rapid increase in overall mutational load suggests that a fraction of matured, pre-existing MBCs was selectively mobilized upon vaccine response and persisted over time.

RBD-specific MBCs from naive individuals obtained 2 months after the boost harbored low mutation numbers in their V_H genes, consistent with the recruitment of naive B cells in the early phase of the vaccine response. It should moreover be noted that MBCs from naive individuals harbor even lower mutational load than MBCs from SARS-CoV-2 recovered patients at a similar 3 months time point after natural infection (**Figure 3E**). This suggests that natural infection might drive a faster maturation process of the MBC response.

RBD-specific ASCs from SARS-CoV-2 recovered patients sorted 7 days after the boost showed clonal relationships with MBCs and highly mutated V_H sequences (**Figure 3F-H and Figure S2A, Table S3F and H**). In contrast, RBD-specific ASCs from naive individuals displayed near germline V_H sequences corresponding to the recruitment of naive B cells in the extra-follicular response (**Figure 3G**). Overall, these results show that the activation of the previously matured pool of MBCs by the mRNA vaccine does not bias the clonal diversity of their repertoire in previously infected individuals, while selectively amplifying MBCs with a higher mutation load.

MBCs mobilized by mRNA vaccine contain high-affinity clones against VOCs.

To determine the potency of the MBC compartment mobilized or elicited by mRNA vaccine against the main natural RBD variants, we first performed ELISA on 1583 supernatants from single-cell culture of sorted RBD-specific MBCs from 4 S-CoV, 4 M-CoV and 3 naive individuals (**Figure 4A, Table S3A**). To normalize for IgG concentration in culture supernatants, we plotted ELISA OD values for WT (Wuhan) vs. B.1.1.7 or B.1.351 RBD variants. Almost all supernatants recognized similarly the WT and B.1.1.7 RBD but 20% of them showed a 10-fold decrease in B.1.351 RBD recognition, with similar frequencies of affected supernatants in SARS-CoV-2 recovered and naive individuals (**Figure 4A-B, Table S2F**).

We next assayed the affinity of MBCs against B.1.1.7, B.1.351, P1, B.1.617.1 and B.1.617.2 RBD variants using Biolayer interferometry (BLI) in which naturally expressed

monoclonal IgG from single-cell culture supernatants were loaded on anti-human IgG biosensors (**Figure S4A**). Monoclonal antibodies expressed by MBCs from recovered patients were highly enriched for high affinity binders against the WT RBD as compared with naive patients ($73.9\pm 5.8\%$ vs $46.5\pm 4.3\%$, $P<0.01$) (**Figure 4C-D**, **Table S2G**), and comparable frequencies were observed against the B.1.1.7 variant. However, overall affinity profiles were no longer different between recovered and naïve donors when the B.1.351, P.1, B.1.617.1 or B.1.617.2 variants were tested, with approximately 20-25% of clones with no or low affinity ($KD>10^{-8}$ M) in both groups (**Figure 4C-D** and **Figure S4B-C**). Somatic hypermutation of V_H genes and antigen-driven affinity maturation against the WT RBD accounts for the higher frequency of high-affinity binders ($KD<10^{-9}$ M) in SARS-CoV-2 recovered compared to naive individuals (**Figure 4E-F**). As expected, the number of V_H mutations showed reduced correlation with affinity against the B.1.351 RBD (**Figure 4E-F**), in line with the selection of these clones against the WT, and not the mutated RBD, during the GC maturation process.

Two by two comparisons of binding affinities between the WT and the different RBD variants allowed us to validate the sensitivity of our approach with nearly all B.1.351 affected monoclonal antibodies (2 fold-increase in variant KD compared to WT KD) also affected in their binding of the P.1 RBD variant sharing similar set of mutations (namely N501Y, E484K and K417T/N) but not of the B.1.1.7 RBD variant which only harbors the N501Y mutation (**Figure 5A**, **5B**). Additional comparisons with B.1.617.1 and B.1.617.2 RBD variants, which both harbor the L452R mutation in addition to E484Q for B.1.617.1 and T478K for B.1.617.2, but not the K417N/T mutation, further revealed cases of antibodies affected in their binding to one or more RBD variants (**Figure S5A-D**). Overall, the natural distribution of mutations in the various VOC RBDs (**Figure 5C**) allowed us to predict the identity of key binding amino acid residues (i.e., N501, K417, E484, L452, T478) within the RBD for 164 out of 382 tested MBC-derived monoclonal antibodies (**Figure 5C-E**). Antibodies affected in their recognition of B.1.351.1, P.1 and B.1.167.1 RBD were identified as binding to E484, with some antibodies using both E484 and L452 for binding, as illustrated by the three-dimensional structure of the RBD (**Figure 5C-E** and **Figure S5A-D**). In agreement with recent structural studies (Yuan et al., 2021), clones recognizing the K417 residue were highly enriched for IGHV3-53 and 3-66 genes, whereas clones recognizing the E484K/Q residue were mostly enriched for the IGHV1-2 and 1-69 genes (**Figure S5E**, **Table S2H**). These results also allowed us to ascribe RBD binding residues of B cells within individual MBC repertoires of naive and recovered patients, confirming the major targeting of the E484 and/or L452 residues within the vaccine activated pool (**Figure 5E**), but also highlighting significant

inter-donor variability in the overall recognition profile of the SARS-CoV-2 RBD by their MBC repertoire.

Affinity maturation and clonal diversity support B.1.351 neutralization by MBCs

Finally, to evaluate the cross-neutralization potential of RBD-specific clones mobilized after vaccination, 279 randomly selected single MBC culture supernatants from S-CoV, M-CoV and naive vaccinated individuals were tested in our focus reduction neutralization assay against authentic D614G and B.1.351 SARS-CoV-2 viruses. The majority of RBD-specific MBCs clones efficiently neutralized D614G but a higher frequency of non-neutralizing clones was observed in naive compared to recovered patients (**Figure 6A and Figure S6A, Table S2I**). Among potent D614G neutralizers, 40-60% of monoclonal antibodies efficiently neutralized B.1.351, without quantitative difference between M-CoV and naive individuals (**Figure 6B**) or clear association with the V_H mutational load or binding affinity to the WT RBD (**Figure 6C and Figure S6A**). Nonetheless, potent neutralizing MBC-derived monoclonal antibodies could be detected in all analyzed donors, including SARS-CoV-2 naive vaccinees (ranging from 5 to 60% of the overall repertoire in the different donors (**Figure S6B**)).

Loss of affinity against B.1.351 RBD mainly affected potent D614G neutralizers (**Figure 6D**), highlighting the strong evolutionary pressure at the virus level to selectively evade this part of the immune response. Plotting KD values for WT vs. B.1.351 RBD among potent D614G neutralizers further revealed four different profiles correlated with B.1.351 neutralization (**Figure 6E**): clones could be classified according to whether or not they retained a similar affinity for binding the B.1.315 RBD compared with the WT one (white and grey sectors, respectively, the grey sector corresponding to lower affinities); among these two categories, clones could be further divided as whether or not they retained neutralization potency against the B.1.315 virus (white and red dots, respectively). Accordingly, MBC-derived monoclonal antibodies displaying similar affinities against both WT and B.1.351 RBD (white sector in **Figure 6E**) were enriched in strong neutralizers against the B.1.351 variant (white dots), but a subset of these antibodies did display reduced neutralization potency (red dots in white sector, **Figure 6F**). These monoclonal antibodies, however, showed a selectively reduced affinity against the whole B.1.351 S ectodomain (**Figure 6G**), suggesting alteration in their binding in the context of the trimeric protein. Among monoclonal antibodies affected in their binding to the B.1.351 RBD (grey sector in **Figure 6E**), maintenance of neutralization activity against the VOC was strongly dictated by their

original affinity against the WT RBD. Whereas clones with weak initial affinity against WT RBD were mostly impaired (red dots in the grey sector), 40% of clones with high initial affinity remained potent neutralizers against the VOC (white dots in the grey sector, **Figure 6E**). This included monoclonals directed against both the E484 and K417 residues of SARS-CoV-2 RBD (**Figure S6C**). This highlights the key role of affinity maturation in shaping the humoral response and anticipating viral escape.

Overall, these results demonstrate that the MBC pool selected by the WT RBD after mRNA vaccination contains, among its diverse and affinity matured repertoire, a substantial fraction of potent neutralizers against VOCs.

Discussion

MBCs display a diverse repertoire allowing for an adaptive response upon re-exposure to the pathogen, especially in the case of variants (Purtha et al., 2011; Weisel et al., 2016). However, repeated antigenic stimulation, either with vaccinations or viral challenge may be deleterious, reducing the diversity of the overall response in which drifted epitopes are less well targeted (Andrews et al., 2015; Mesin et al., 2020). Thus, understanding how mRNA vaccination impacts the MBC pool shaped by a previous exposure to SARS-CoV-2 and to determine its capacity to neutralize variants is critical. More generally, to decipher how MBCs from naive vaccinees differ and evolve in comparison with SARS-CoV-2 recovered patients is also of major importance in the pandemic context.

We report here a longitudinal study of SARS-CoV-2 recovered patients, followed over one year after their initial infection and vaccinated with the BNT162b2 mRNA vaccine. The vaccine response of SARS-CoV-2 naive individuals was analyzed in parallel. The strength of our approach is the large scale, unbiased study of the MBC response against SARS-CoV-2 at the single cell scale using *in vitro* activation of randomly sampled memory/activated B cells. This allowed a deep functional analysis, which included affinity assessment against WT RBD and against 5 variants including B.1.617.2, and determination of neutralization potency of these secreted IgG against two SARS-CoV-2 viruses, without cloning and re-expression intermediates. We focused on the RBD because anti-RBD antibodies contribute to the majority of neutralizing antibodies and its mutations allow for immune escape of VOC (Ju et al., 2020; Robbiani et al., 2020), together with additional targets in the N-terminal domain of the Spike (McCallum et al., 2021).

Our study highlights the stability of the overall RBD-specific MBC population up to 12 months after infection with a stable mutation profile, extending observations on memory persistence in COVID-19 (Wang et al., 2021b). Dynamics of RBD-specific cells after mRNA vaccination in SARS-CoV-2 recovered patients reflect the plasticity of the MBC pool, which promptly and widely activates, proliferates and generates ASCs, and then contracts as resting MBCs (Goel et al., 2021; Reynolds et al., 2021; Wang et al., 2021b). This mobilized population contains highly mutated affinity-matured clones that settle, expand and persist for up to 2 months after the boost with a higher frequency and mutational load than before the vaccinal boost. Despite this, longitudinal VDJ sequencing revealed a limited impact on the diversity of this previously matured repertoire. Thus, the expansion of the MBC pool does not seem to impair archives of the B cell specificities that have been selected during the amplification. In contrast, and mirroring early stages of the extrafollicular response after

infection (Woodruff et al., 2020), RBD-specific B cells expressing near germline recurrent V_H genes with potent affinity are recruited after mRNA vaccination in naive individuals. MBC from naive individuals also acquired somatic mutations with time but harbored, 2 months after the boost, fewer mutations than SARS-CoV-2 recovered patients 3 months after COVID-19. Thus, whereas the MBC pool progressively matures in naive vaccinees, its maturation and amplification were less pronounced, resulting in less RBD-specific MBCs compared to SARS-CoV-2 recovered patients at 12 months after infection (respectively 7.8 and 3 times less than S-CoV and M-CoV) and 2 months after the boost (respectively 18.2 and 6 times less than S-CoV and M-CoV).

As previously reported, most sera of SARS-CoV-2 recovered patients efficiently neutralized the B.1.351 variant after mRNA vaccine, which contrasted with the significant lower neutralization potency of the sera of naive vaccinated individuals (Goel et al., 2021; Reynolds et al., 2021; Stamatatos et al., 2021; Wang et al., 2021b). This likely reflects the quality and maturation of the B cell pool mobilized by the vaccine, i.e. an extrafollicular response in naive vaccinees and a mature MBC response in recovered patients.

A fraction of recurrent and convergent V_H genes of MBCs failed to recognize the B.1.351 variant RBD in both cohorts but a large proportion of clones retained high affinity against this variant. This is consistent with a recent report showing that B cell clones expressing potent antibodies are selectively retained in the repertoire over time (Wang et al., 2021b). This phenomenon occurs independently of the mutational load, high-affinity clones against variants being “randomly” present in the MBC repertoire of SARS-CoV-2 recovered or naive individuals. So, despite the fact that amplitude and quality of the MBC response after mRNA vaccine appears to be lower in naive than in previously infected individuals, high-affinity clones with neutralizing potency against VOC settle in their repertoire, suggesting that their MBC pool could compensate for the time-dependent decay of the initial antibody response.

Correlation of neutralization and affinity shows a complex profile for antibodies expressed by MBCs. Immune escape can affect high-affinity clones against WT RBD, but at the same time, a proportion of clones with high affinity for WT RBD maintain neutralizing potency against B.1.351, contrasting with clones with low or weak affinity that constantly failed to neutralize variants. It indicates that high affinity provides some flexibility for antibodies to cope with mutations affecting their binding target and to conserve their neutralization potency. Consistent with structural analysis (Yuan et al., 2021), determination of targeted epitopes using binding of different RBD of VOC shows that E484 preferentially

affected the binding affinity of the IGHV1-2/1-69 genes, and K417N and N501Y the one of IGHV3-53/3-66 and IGHV1-2. It underlines that, if particular antibody lineages are affected by RBD mutations, others may retain neutralizing properties (Barnes et al., 2020; Greaney et al., 2021, 2021b; Muecksch et al., 2021; Scheid et al., 2021; Wang et al., 2021b).

Altogether, these data describe an immune response maturing with time in SARS-CoV-2 convalescent patients, and resulting in a massive, high-affinity response after vaccination, which, even imprinted by the Wuhan-type RBD, displays an improved recognition of the RBD variants as well. In this immune evolution scheme, the response of naive vaccinees nevertheless lags behind the maturation process that took place during infection. As recently proposed, vaccinated individuals will further improve with time the affinity and diversity of their MBC response and therefore probably also improve their quantitative and qualitative antibody response through the persistence of vaccine-induced germinal centers (Cho et al., 2021; Turner et al., 2021). Nonetheless, our observations in SARS-CoV-2 recovered patients suggest that repeated challenges, even using the original spike protein, will help to reduce any persisting differences and allow vaccinated people to respond more efficiently to current SARS-CoV-2 variants by recall of affinity-matured MBCs.

Limitations of the study

The relatively small size and the limited follow-up of the cohorts do not allow us to identify characteristics of the patients that would predict response to mRNA vaccine and its persistence. Furthermore, patients with severe form of Covid-19 were not matched for age and comorbidities with those who presented a mild form or with naive individuals, thus differences between these groups must be interpreted with caution. Finally, we focused our study on the RBD domain of the SARS-CoV-2 spike protein as it represents the major known target for neutralizing antibodies. However, neutralizing antibodies against other domains of the trimeric spike have been described, notably against the N-terminal domain (NTD). Larger cohorts of individuals with a wider spectrum of age and comorbidities, extended follow-up (up to 6 months or more) and dedicated studies on non RBD-specific neutralizing MBCs would be important in the future to provide a comprehensive picture of B cell memory responses directed against VOCs after mRNA vaccination.

Acknowledgments:

We thank Garnett Kelsoe for providing us with the human cell culture system, together with invaluable advices. We thank A. Boucharlat and the Chemogenomic and Biological screening core facility headed by F. Agou, as well as P. England and the Molecular Biophysics core facility at the Institut Pasteur, Paris, France for support during the course of this work. We also thank Sébastien Storck, Lucie Da Silva, Sandra Weller for their advices and support; we thank the physicians, Constance Guillaud, Raphael Lepeule, Frédéric Schlemmer, Elena Fois, Henri Guillet, Nicolas De Prost, Pascal Lim, whose patients were included in this study. Graphical abstract, Figure 1A and Figure S4A were created using Biorender.com

Funding: This work was initiated by a grant from the Agence Nationale de la Recherche and the Fondation pour la Recherche Médicale (ANR, MEMO-COV-2 -FRM), and funded by the Fondation Princesse Grace and by an ERC Advanced Investigator Grant (B-response). Assistance Publique – Hôpitaux de Paris (AP-HP, Département de la Recherche Clinique et du Développement) was the promotor and the sponsor of MEMO-COV-2. Work in the Unit of Structural Virology was funded by Institut Pasteur, Urgence COVID-19 Fundraising Campaign of Institut Pasteur. A.S. was supported by a Poste d'Accueil from the Institut National de la Santé et de la Recherche Médicale (INSERM), I.F. by a fellowship from the Agence Nationale de Recherches sur le Sida et les Hépatites Virales (ANRS), M.B. by a CIFRE fellowship from the *Association Nationale de la recherche et de la technologie* (ANRT) and A.DLS by a SNFMI fellowship. P.B. acknowledges funding from ANR (ANR-14-CE16-0011 - DROPmAbs), by the Institut Carnot Pasteur Microbes et Santé (ANR 11 CARN 0017-01), the Institut Pasteur and INSERM.

Author contributions: Conceptualization: P.C., A.S., J.C.W., C.A.R., and M.M.; Data curation: P.C., A.S., M.B., G.B.S., I.A. Formal Analysis: A.S., P.C., M.B., G.B.S., I.A., M.Bo.; A.DLS, A.V., S.F., I.F.; Funding acquisition: S.F., J.C.W., C.A.R., and M.M.; Investigation: A.S., P.C., A.DLS., I.A., A.V.; Methodology: A.S., J.C.W., C.A.R., P.C. and M.M.; Project administration: P.C., F.C.P., J.C.W., C.A.R., and M.M.; Resources: J.M.P., F.N.P., S.F., E.C., L.G., Ma.Mi., B.G., S.G., G.M., Y.NG., V.Z., P.B., F.R., C.A.R., M.M.; Software: P.C.; Supervision: P.C., J.C.W., C.A.R., P.B., F.R. and M.M.; Validation: A.S., I.A., A.V., A.DLS, M.B., C.A.R., P.C., M.M.; Visualization: P.C., A.S., I.A., A.DLS., M.M.; Writing – original draft: P.C., A.S., J.C.W., C.A.R., and M.M.; Writing – review & editing: all authors.

Journal Pre-proof

Figure 1. mRNA vaccine boosts humoral response against SARS-CoV-2 and VOCs in naive and SARS-CoV-2 recovered patients.

(A) Cohort design (B) Anti-SARS-CoV-2 RBD serum IgG titers measured by ELISA in S-CoV (n=16, left panel, dark blue) and M-CoV (n=15, right panel, light blue) at 6 (M6) and 12 months (M12) post symptom onset. (C) Evolution of the anti-SARS-CoV-2 RBD serum IgG titers after BNT162b2 vaccination. IgG titers (arbitrary units, AU) are shown at pre-boost (M6 or M12) for SARS-CoV-2 recovered (S-CoV: dark blue; M-CoV: light blue) or after the prime for naive patients (white), as well as 7 days and 2 months after the vaccine boost. Bars indicate mean \pm SEM. The lower dashed line (B-C) indicates the positivity threshold and the upper dashed line indicates the upper limit of detection as provided by the manufacturer. (D) Heatmap representing the observed in vitro neutralization of D614G SARS-CoV-2 (left), B.1.351 (middle) and B.1.617.2 VOCs (right) by sera from SARS-CoV-2 recovered patients at the pre-boost and boost + 2 months time points (serial dilutions: 1/10, 1/40, 1/160, 1/640, 1/2560, 1/10240). Each line represents one patient. (E) Half maximal inhibitory concentration (IC₅₀) for all sera tested from SARS-CoV-2 recovered and naive patients at pre-boost and boost + 2 months time points against D614G SARS-CoV-2, B.1.351 and B.1.617.2 VOCs. Bars indicate mean \pm SEM. (B) Two-way ANOVA with multiple comparisons of all groups; (C) Repeated measures mixed effects model analysis with two sets of multiple comparisons (between donor groups inside each time-point and between time points for each donor group) and (E) repeated measures mixed effects model analysis with multiple comparisons between time points for each recovered donor group and Kruskal-Wallis with multiple comparisons between donor groups inside each time-point were performed (Benjamini, Krieger and Yekutieli FDR correction was used for all multiple comparisons). (****P<0.0001, ***P<0.001, **P < 0.01, *P < 0.05). See also Figure S1 and Table S1.

Figure 2. mRNA vaccination activates multiple SARS-CoV-2 RBD-specific B cell subsets in SARS-CoV-2 recovered and naive patients.

(A) Representative dot-plot of SARS-CoV-2 RBD-staining of CD19⁺IgD⁻CD27⁺CD38^{int/-} MBCs at 6 (M6) and 12 months (M12) in one S-CoV and one M-CoV representative patients. (B-C) Frequencies of SARS-CoV-2 RBD-specific cells in live CD19⁺IgD⁻CD27⁺CD38^{int/-} MBCs at 6 and 12 months post symptom onset in SARS-CoV-2 recovered patients (S-CoV; dark blue, n=14/14; M-CoV: light blue, n=11/12) (B) and at pre-boost, boost + 7 days and boost + 2 months time points in S-CoV (dark blue, n=17/6/6), M-CoV (light-blue, n=14/21/20) and naive (white, n=10/13/23) patients. Bars indicate mean \pm SEM. (D) UMAP

projections of concatenated CD19⁺IgD⁻ B cells multi-parametric FACS analysis from 5 S-CoV and 8 M-CoV patients analyzed longitudinally. His-tagged labeled SARS-CoV-2 RBD-specific cells are overlaid as red dots. **(E-F)** Unsupervised clustering (FlowSOM) performed on the concatenated FACS dataset. Main defined clusters (>2% of total CD19⁺IgD⁻ B cells) are shown as overlaid contour plots on the global UMAP representation (E). Cluster distribution of SARS-CoV-2 RBD-specific cells in identified clusters, at indicated time point, is further displayed as bar plots (F). Bars indicate mean±SEM. **(G)** Representative dot plots for CD71 and CD19 expression in IgD⁻CD19⁺CD38^{int/-} B cells at indicated time points from representative S-CoV, M-CoV and naive patients. SARS-CoV-2 RBD-specific MBCs are overlaid as red dots. **(H)** Frequencies of SARS-CoV-2 RBD-specific cells displaying an activated B cell (CD19⁺CD27⁺IgD⁻CD71⁺) phenotype at indicated time points. **(I)** Proportion of Spike-specific MBCs recognizing RBD in each individual at the two-month time point. Bars indicate mean±SEM. **(B)** Two-way ANOVA with multiple comparisons of all groups; **(C** and **H)** Repeated measures mixed effects model analysis with two sets of multiple comparisons (between donor groups inside each time-point (black lines) and between time points for each donor group (colored lines)) and **(I)** ordinary one-way ANOVA were performed (Benjamini, Krieger and Yekutieli FDR correction was used for all multiple comparisons). Only significant comparisons are highlighted in panels (C, H, I). (***)P<0.0001, (***) P<0.001, (**P < 0.01, *P < 0.05). See also Figure S2 and Table S2.

Figure 3. mRNA vaccination elicits a diverse RBD-specific memory B cell repertoire in SARS-CoV-2 recovered and naive patients.

(A) Experimental scheme for the functional assessment of naturally expressed monoclonal antibodies from RBD-specific MBCs. **(B-C)** Pie charts representing the clonal distribution of RBD-specific MBCs sorted from 2 S-CoV and 2 M-CoV at pre-boost, boost + 7 days and boost + 2 months time points **(B)** and 2 naive patients at boost + 2 months **(C)**. Clonal representation is depicted according to Wang et al. (2021b): colored slices indicate an expanded MBC clone (2 or more sequences at a given time-point) found at several time-points in the same patient (persistent clone) or in clonal relationship with ASCs at boost + 7 days; grey slices indicate an expanded MBC clone found at a single time-point; white slices indicate unique sequences found at several time points. The main white sector in each pie chart represents unique sequences, observed at a single time point. Outer black semi-circular line indicates the proportion of sequences belonging to expanded clones at a given time point. The total number of sequences is indicated at the pie center. **(D)** Circos plot showing clonal

relationships between all sequenced RBD-specific MBCs grouped by donors and time-points. Blue lines connect persistent clones and grey lines connect clones shared by at least two donors (public clones). **(E)** Violin plots showing the number of mutations in the V_H segment of RBD-specific MBCs at successive time points in SARS-CoV-2 recovered (M3 = 81 sequences; M6 = 600, M12 = 109, Boost + 7 days = 930, Boost + 2 months = 430) and naive donors (Boost + 2 months = 151). Red line indicates median. **(F)** Pie chart representing the clonal distribution of RBD-specific ASCs sorted for 2 SARS-CoV-2 recovered and 2 naive patients at boost + 7 days. Colored slices indicate a clone in clonal relationship with an expanded MBCs clone from the same donor, grey slices indicate an expanded ASC clone not found in MBCs from the same donor and white slices indicate unique ASC sequences in clonal relationship with a non-expanded MBC clone. Outer black semi-circular line indicates the proportion of sequences belonging to expanded ASC clones. The total number of sequences is indicated at the pie center. **(G)** Violin plots showing the number of mutations in the V_H segment of RBD-specific ASCs sorted from 2 SARS-CoV-2 recovered (n= 86 sequences) and 2 naive donors (n= 49 sequences) at boost + 7 days. Red line indicates median. **(H)** Circos plot showing clonal relationships between RBD-specific MBCs (white mid-semi-circular slice) and RBD-specific ASCs (green mid-semi-circular slice) sorted at boost + 7 days from 2 SARS-CoV-2 recovered (one S-CoV, one M-CoV, dark blue outer circular slice) and 2 naive (white outer circular slice). Blue lines indicate shared clones between ASCs and MBCs and grey lines indicate public clones containing ASCs. Ordinary one-way ANOVA with multiple comparisons (Benjamini, Krieger and Yekutieli FDR correction) (G) and a two-tailed Mann-Whitney test (E) were performed (****P<0.0001). See also Figure S3 and Table S2.

Figure 4. The memory B cell pool of vaccinated individuals contains high-affinity clones against WT SARS-CoV-2 and B.1.1.7 and B.1.351 VOCs.

(A) WT RBD versus B.1.1.7 RBD (left) or B.1.351 RBD ELISA values (right) for all single-cell culture supernatants of RBD-specific MBCs isolated from SARS-CoV-2 recovered (dark blue, n=952) and naive (white, n=373) donors. Only supernatants with WT ELISA OD/blank ratio ≥ 5 are displayed. The red sector identifies naturally expressed antibodies defined as impaired in the recognition of a given variant (variant ELISA OD/blank ratio < 3 or ≥ 10 -fold decrease in variant recognition). **(B)** Frequencies of single RBD-specific MBC culture supernatants with functional or impaired recognition of B.1.1.7 or B.1.351 RBD variants as assessed by ELISA. **(C)** Dissociation constants (KD, expressed as moles/L) measured by bio-

layer interferometry for 382 naturally expressed monoclonal antibodies against WT, B.1.1.7 and B.1.351 RBD. Tested monoclonal antibodies were randomly selected from single-cell culture supernatants of RBD-specific MBCs isolated from SARS-CoV-2 recovered (n=251) and naive donors (n=131) and displaying WT RBD ELISA OD/blank ratio ≥ 3 . Background colors define high ($KD < 10^{-9}$ M), mid ($10^{-9} \leq KD < 10^{-8}$ M) and low ($10^{-8} \leq KD < 10^{-7}$) affinity monoclonal antibodies. All monoclonal antibodies with no measurable affinity ($KD \geq 10^{-7}$) were considered non-binders. **(D)** Histogram showing the intra-donor binding affinity distribution of monoclonal antibodies tested against WT, B.1.1.7 and B.1.351 RBD variants, as defined in **(C)**, for SARS-CoV-2 recovered or naive donors. Bars indicate mean \pm SEM. **(E)** Measured KD (M) against WT (left) or B.1.351 RBD (right) vs. number of V_H mutations for all tested monoclonal antibodies with available V_H sequence from SARS-CoV-2 recovered (dark blue, n=249) and naive (white, n=114) donors (Spearman correlations for all sequences: V_H mutation/WT KD: $r = 0.3791$, $P < 0.0001$; V_H mutation/B.1.351 KD: $r = 0.152$, $P = 0.0033$). **(F)** Pie chart showing the binding affinity distribution of all tested monoclonal antibodies with low (<10 mutations, upper panel) or high V_H mutation numbers (>10, lower panel) against WT, B.1.1.7 and B.1.351 RBD variants as defined in **(C)**. Numbers at center of the pie chart indicate the total number of tested monoclonal antibodies in each group. **(C)** A two-way ANOVA with two sets of multiple comparisons (between tested variants inside each group (black lines) and between groups for each tested variants (colored lines)) was performed (Benjamini, Krieger and Yekutieli FDR correction). (**** $P < 0.0001$, ** $P < 0.01$, * $P < 0.05$). See also Figure S4 and Table S2.

Figure 5. Variant RBD recognition profile reveals key residues recognized by memory B cells mobilized by the mRNA vaccine boost.

(A) Dot plot representing the KDs for B.1.351 RBD versus WT RBD for all tested monoclonal antibodies from SARS-CoV-2 recovered (dark blue dots) and naive donors (white dots). The red shaded zone indicates B.1.351-affected monoclonal antibodies, defined as those with at least two-fold increased KD for B.1.351 as compared to WT RBD. **(B)** Dot plots representing the KDs for B.1.1.7, P.1, B.1.617.1 and B.1.617.2 RBD versus WT RBD. B.1.351 affected monoclonal antibodies are highlighted as larger size red dots (corresponding to clones present in the red sector in **(A)**). Percentages indicate the proportion of B.1.351 affected monoclonal antibodies also affected by the indicated RBD variant. **(C)** Distribution of known mutations in the RBD domain between B.1.1.7, B.1.351, P.1, B.1.617.1 and

B.1.617.2 SARS-CoV-2 variants. **(D)** RBD (extracted from the PDB:6XR8 spike protein trimer structure) shown in three orthogonal views with the ACE2 receptor binding motif highlighted in yellow and the residues found mutated in a least one of the tested variants - L452, K417, T478, E484 and N501- highlighted in black. Single or group of predicted binding residues are further highlighted by colored ovals according to the color scheme used in (E). **(E)** Frequencies of predicted essential binding residues, as defined by RBD variants recognition profile in BLI, for all monoclonal antibodies isolated from each of the 11 tested donors. Numbers of tested monoclonal antibodies for each donor are indicated on top of each histogram. See also Figure S5 and Table S2.

Figure 6. A substantial proportion of memory B cells in vaccinated individuals neutralizes D614G SARS-CoV-2 and B.1.351 VOC.

(A) Pie charts showing the proportion of single-cell culture supernatants of RBD-specific MBCs isolated from SARS-CoV-2 recovered (S-CoV, n=104; M-CoV, n=123) and naive donors (n=52) displaying potent, weak or no neutralization potential (none) against D614G SARS-CoV-2 and B.1.351 SARS-CoV-2 variant. Potent neutralizers are defined as >80% neutralization at 16 nM, weak neutralizer as neutralization <80% at 16 nM but >80% at 80 nM. Others were defined as non-neutralizing. **(B)** Histogram showing the proportion of B.1.351 SARS-CoV-2 potent, weak and non-neutralizing single-RBD-specific MBC culture supernatants grouped based on their neutralization potency against D614G SARS-CoV-2. **(C)** Heatmap showing the in vitro neutralization of D614G SARS-CoV-2 and B.1.351 variant at 80 nM and 16 nM for all culture supernatants whose monoclonal antibodies were also tested in BLI against all variants (S-CoV, n=85; M-CoV, n=67 and naive, n=27). KD (M) against WT, B.1.351 and B.1.617.2 RBD for each monoclonal antibody are represented on top along with predicted binding residues. **(D)** Ratio of WT over B.1.351 RBD KD for all monoclonal antibodies displayed in (C), grouped based on their neutralization potency against D614G SARS-CoV-2. **(E)** KD (M) against B.1.351 versus WT RBD for all D614G SARS-CoV-2 potent neutralizers monoclonal antibodies. Dot color indicates the neutralization potency against B.1.351 SARS-CoV-2 variant. Grey shade highlights binding-impaired clones against the B.1.351 RBD variant as defined in Figure 4G. **(F)** B.1.351 SARS-CoV-2 neutralization potency distribution of all tested potent D614G SARS-CoV-2 neutralizers, grouped based on their affinity for WT RBD and affinity loss against B.1.351. **(G)** WT versus B.1.351 variant RBD or Spike KD ratio for selected monoclonal antibodies showing no clear B.1.351 RBD binding impairment and no loss (left) or clear loss (right) of neutralization potency against the

B.1.351 SARS-CoV-2 variant. (G) A paired Wilcoxon test was performed (**** $P < 0.0001$).
See also Figure S6 and Table S2.

Journal Pre-proof

STARMethods

RESOURCE AVAILABILITY

Lead Contact

Further information and requests for resources and reagents should be directed to and will be fulfilled by the Lead Contact, Matthieu Mahévas (matthieu.mahevas@aphp.fr).

Materials Availability

No unique materials were generated for this study.

Data and Code Availability

- Single cell culture VDJ sequencing data reported in **Figure 3 and Figure S3** are directly included in this study as part of **Table S3**. Additional Supplemental items are available from Mendeley Data at <https://data.mendeley.com/datasets/4jfnn6xt/1>
- This paper does not report original code.
- Any additional information required to reanalyze the data reported in this paper is available from the lead contact upon request.

EXPERIMENTAL MODEL AND SUBJECT DETAILS

Study participants

In total, 43 patients with recovered COVID-19 (17 S-CoV and 26 M-CoV) and 25 naïve patients were included in this study and sampled at least one time before boost vaccination (12 months post infection for recovered or after the prime for naïve) or after boost vaccination (boost + 7 days or boost + 2 months). Among the 43 SARS-CoV-2 recovered patients, 34 were from the original MEMO-COV-2 cohort and followed up to 12 months post-infection and/or vaccination. Seventeen of these patients had severe COVID-19 (patients requiring oxygen, S-CoV) and 17 had a mild COVID-19 disease (mainly healthcare workers, M-CoV). An additional cohort of 9 patients who also experienced mild COVID-19 during the first wave of pandemic in France and were vaccinated at least six months after the infection were specifically recruited for this study. SARS-CoV-2 infection was defined as confirmed reverse transcriptase polymerase chain reaction (RT-PCR) on nasal swab or clinical presentation associated with typical aspect on CT-scan and/or serological evidence. Twenty-five healthcare

workers who had no history of COVID-19 and negative IgG anti- nucleocapsid (and/or Spike) were enrolled in the naive group (IRB 2018-A01610-55). Detailed information on the individuals, including gender and health status, can be found in Table S1.

All vaccinated subjects received the BNT162b2 mRNA vaccine. SARS-CoV-2 recovered patients received only one dose, in line with French guidelines, except 3 who received 2 doses (See **Table S1**). First injection was realized in mean 309 days (\pm SD 44.6 days) after the infection. Naive patients received two doses at a mean 27.7 days (\pm SD 1.8 days) interval.

Prior to vaccination, samples were collected from SARS-CoV-2 recovered patients 12 months post symptoms onset (mean \pm SD: 329.1 \pm 15.8 days after disease onset for S-CoV, and 342.0 \pm 8.6 days after disease onset for M-CoV). Samples at 12 months post disease onset were defined as “pre-boost”. For patients not sampled before vaccination (n=9/34), sample at 6 months was considered as “pre-boost”. For SARS-CoV-2 naive patients, the "prime" time-point was defined as the sampling between the two doses and was drawn at a mean 20.2 \pm 5.9 days after the first injection.

Samples were additionally collected shortly after the boost (mean \pm SD: 10 \pm 5.3 days for S-CoV; 23 \pm 6.1 days for M-CoV and 9 \pm 4.0 days for naive), and 2 months after the boost (mean \pm SD: 64.7 \pm 15.3 days for S-CoV ; 63.2 \pm 11.9 days for M-CoV and 63.3 \pm 9.0 days for naive). Clinical and biological characteristics of these patients are summarized in **Table S1**. Patients were recruited at the Henri Mondor University Hospital (AP-HP), between March and April 2021. MEMO-COV-2 study (NCT04402892) was approved by the ethical committee Ile-de-France VI (Number: 40-20 HPS), and was performed in accordance with the French law. Written informed consent was obtained from all participants.

Virus strains

The reference D614G strain (hCoV-19/France/GE1973/2020) and the B.1.351 strain (CNR 202100078) were supplied by the National Reference Centre for Respiratory Viruses hosted by Institut Pasteur and headed by Sylvie van der Werf. The B.1.617.2 SARS-CoV2-variant Delta/2021/I7.2 200 (GISAID ID: EPI_ISL_2029113) was supplied by the Virus and Immunity Unit hosted by Institut Pasteur (Paris, France) and headed by Olivier Schwartz (Planas et al., 2021b). The viral strains were supplied through the European Virus Archive goes Global (EVAg) platform, a project that has received funding from the European Union’s Horizon 2020 research and innovation program under grant agreement number 653316.

D614G, B.1.351, and B.1.617.2 viral stocks were prepared by amplification and titration in Vero E6 cells and were used at passage 3 and passage 2 respectively. Single use aliquots stored at -80°C were used for all the assays.

METHOD DETAILS

Anti- RBD (S) SARS-CoV-2 antibodies assay

Serum samples were analyzed for anti-S-RBD IgG titers with the SARS-CoV-2 IgG Quant II assay (ARCHITECT®, Abbott Laboratories). The latter assay is an automated chemiluminescence microparticle immunoassay (CMIA) that quantifies anti-RBD IgG, with 50 AU/mL as a positive cut-off and a maximal threshold of quantification of 40,000 AU/mL. All assays were performed by trained laboratory technicians according to the manufacturer's standard procedures.

Recombinant protein purification

Construct design

The ectodomain from the SARS-CoV-2 Spike (residues 1-1208) was designed as a stabilized construct with six proline mutations (F817P, A892P, A899P, A942P, K986P, V987P), a GSAS substitution at the furin cleavage site (residues 682–685) and a C-terminal Foldon trimerization motif (Hsieh et al, 2020), followed by Hisx8, Strep and Avi tags. This construct was cloned using its endogenous signal peptide in pcDNA3.1(+).

The SARS-CoV-2 Receptor Binding Domain (RBD) was cloned in pcDNA3.1(+) encompassing the Spike (S) residues 331-528, and it was flanked by an N-terminal IgK signal peptide and a C-terminal Thrombin cleavage site followed by Hisx8, Strep and Avi tags. The mutations present on the B.1.1.7 (N501Y), B.1.351 (K417N, E484K, N501Y), P.1 (K417T, E484K, N501Y), B.1.617.1 (L452R, E484Q) and B.1.617.2 (L452R, T478K) variants were introduced by PCR mutagenesis using standard methods.

Protein expression and purification

Plasmids coding for recombinant proteins were transiently transfected in Expi293F™ cells (Thermo Fischer) using FectoPRO® DNA transfection reagent (Polyplus), according to the manufacturer's instructions. Cells were incubated at 37 °C for 5 days and then the culture was centrifuged and the supernatant was concentrated. Proteins were purified from the supernatant by affinity chromatography using StrepTactin columns (IBA) (SARS-CoV-2 S) or His-Trap™ Excel columns (Cytiva) (SARS-CoV-2 RBD). A final step of size-exclusion chromatography (SEC) in PBS was also performed, using either a Superose6 10/300 column

(Cytiva) for the SARS-CoV-2 S, or a Superdex200 10/300 (Cytiva) for the SARS-CoV-2 RBD.

Flow cytometry and cell sorting

PBMCs were isolated from venous blood samples via standard density gradient centrifugation and used after cryopreservation at -150°C . Cells were thawed in RPMI-1640 (Gibco)-10% FBS (Gibco), washed twice and incubated with $5\ \mu\text{g}$ of the SARS-CoV-2 His-tagged spike protein or WT RBD in $100\ \mu\text{L}$ of PBS (Gibco)-2% FBS during 20 min on ice. For each condition, 2.5×10^6 cells were washed and resuspended in the same conditions, then the fluorochrome-conjugated antibody cocktail including the 2 anti-His antibodies was added at pre-titrated concentrations (1:100 for CD19, CD21, CD11c, CD71, CD38, CD3, CD14 and IgD, 1:50 for CD27 and 1:33 for anti-His tag) for 20 min at 4°C and viable cells were identified using a LIVE/DEAD Fixable Aqua Dead Cell Stain Kit (Thermo Fisher Scientific, 1:200) incubated with conjugated antibodies. Samples were acquired using a LSR Fortessa SORP (BD Biosciences). For cell sorting, cells were stained using the same protocol and then sorted in 96 plates using the ultra-purity mode on a MA900 cell sorter (SONY), or Aria III (BD Biosciences). Data were analyzed with FlowJo or Kaluza softwares. Detailed gating strategies for individual markers are depicted in Figure S1.

For UMAP generation and visualization (**Figure 2**), FCS files from 5 S-CoV, 8 M-CoV and 4 naive patients with complete panel acquisition at pre boost, boost + 7 days and boost + 2 months (**Table S1**) were concatenated. The UMAP (v3.1) plugin in FlowJO was used to calculate the UMAP coordinates for the resulting 536.161 cells (with 30 neighbors, metric = euclidian and minimum distance = 0.5 as default parameters). The FlowSOM (v2.6) plugin was used in parallel on the same downsampled dataset to create a self-organizing map (using $n = 10$ clusters as default parameter). This self-organizing map was then applied to the initial FCS files to calculate both total and RBD-specific MBC repartition in identified clusters on all collected cells for each donor. Naive patients were not further analyzed due to the very low number of RBD specific B cells. Both UMAP and FlowSOM plugin were run on viable dump⁻ CD19⁺ IgD⁻ cells taking into account fluorescent intensities from the following parameters: FSC-A, SSC-A, CD19, CD21, CD11c, CD71, CD38, CD27 and IgD, while excluding the dump (CD3 and CD14), viability and RBD channels. Contour plots (equal probability contouring, with intervals set to 5% of gated populations) for each identified cluster were further overlaid on UMAP projection in FlowJO. For visualization purposes,

only the outermost density representing 95% of the total gated cells was kept for the final figure, all other contour lines were removed in Adobe Illustrator.

Single-cell culture

Single cell culture was performed as previously described (Crickx et al., 2021). Single B cells were sorted in 96-well plates containing MS40L^{lo} cells expressing CD40L (kind gift from G. Kelsoe, Luo et al., 2009). Cells were co-cultured at 37°C with 5% CO₂ during 21 or 25 days in RPMI-1640 (Invitrogen) supplemented with 10% HyClone FBS (Thermo Scientific), 55 µM 2-mercaptoethanol, 10 mM HEPES, 1 mM sodium pyruvate, 100 units/mL penicillin, 100 µg/mL streptomycin, and MEM non-essential amino acids (all Invitrogen), with the addition of recombinant human BAFF (10 ng/ml), IL2 (50 ng/ml), IL4 (10 ng/ml), and IL21 (10 ng/ml; all Peprotech). Part of the supernatant was carefully removed at days 4, 8, 12, 15 and 18 and the same amount of fresh medium with cytokines was added to the cultures. After 21 days of single cell culture, supernatants were harvested and stored at -20°C. Cell pellets were placed on ice and gently washed with PBS (Gibco) before being resuspended in 50 µL of RLT buffer (Qiagen) supplemented with 1% 2-mercaptoethanol and subsequently stored at -80°C until further processing.

ELISA

Total IgG and SARS-CoV-2 WT RBD, B.1.1.7 RBD and B.1.351 RBD-specific IgG from culture supernatants were measured using homemade ELISA. 96 well ELISA plates (Thermo Fisher) were coated with either goat anti-human Ig (10 µg/ml, Invitrogen) or recombinant SARS-CoV-2 WT RBD, B.1.1.7 RBD or B.1.351 RBD protein (2.5 µg/ml each) in sodium carbonate during 1h at 37°C. After plate blocking, cell culture supernatants were added for 1hr, then ELISA were developed using HRP-goat anti-human IgG (1 µg/ml, Immunotech) and TMB substrate (Eurobio). OD450 and OD620 were measured and Ab-reactivity was calculated after subtraction of blank wells. Supernatants whose ratio of OD450-OD620 over control wells (consisting of supernatant from wells that contained spike-negative MBCs from the same single cell culture assay) was over 3 were considered as positive for WT RBD, B.1.1.7 RBD or B.1.351 RBD ELISA. PBS was used to define background OD450-OD620.

Single-cell IgH sequencing

Clones whose culture had proven successful (IgG concentration ≥ 1 µg/mL at day 21-25) were selected and extracted using the NucleoSpin96 RNA extraction kit (Macherey-Nagel) according to the manufacturer's instructions. A reverse transcription step was then performed

using the SuperScript IV enzyme (ThermoFisher) in a 14 μ l final volume (42°C 10 min, 25°C 10 min, 50°C 60 min, 94°C 5 min) with 4 μ l of RNA and random hexamers (ThermoFisher scientific). A PCR was further performed based on the protocol established by Tiller et al (Tiller et al., 2008). Briefly, 3.5 μ l of cDNA was used as template and amplified in a total volume of 40 μ l with a mix of forward L-VH primers (**Table S3**) and reverse C γ primer and using the HotStar® Taq DNA polymerase (Qiagen) and 50 cycles of PCR (94°C 30 s, 58°C 30 s, 72°C 60 s). PCR products were sequenced with the reverse primer CHG-D1 and read on ABI PRISM 3130XL genetic analyzer (Applied Biosystems). Sequence quality was verified using CodonCode Aligner software (CodonCode Corporation).

For specific patients and time points (see **Table S1**), some IgH sequences were obtained directly from single-cell sorting in 4 μ L lysis buffer containing PBS (Gibco), DTT (ThermoFisher) and RNAsin (Promega). Reverse transcription and a first PCR was performed as described above (50 cycles) before a second 50-cycles PCR using 5' AgeI VH primer mix and C γ -CH1 3' primer, before sequencing.

Computational analyses of VDJ sequences

Processed FASTA sequences from cultured single-cell V_H sequencing were annotated using Igbblast v1.16.0 against the human IMGT reference database. Clonal cluster assignment (DefineClones.py) and germline reconstruction (CreateGermlines.py) was performed using the Immcantation/Change-O toolkit (Gupta et al., 2015) on all heavy chain V sequences. Sequences that had the same V-gene, same J-gene, including ambiguous assignments, and same CDR3 length with maximal length-normalized nucleotide hamming distance of 0.15 were considered as belonging to the same clonal group. Mutation frequencies in V genes were then calculated using the calcObservedMutations() function from the Immcantation/SHazaM v1.0.2 R package. VH repartitions and Shannon entropies were calculated using the countGenes() and alphaDiversity() functions from the Immcantation/alakazam v1.1.0 R package. Further clonal analyses on all productively rearranged sequences were implemented in R. Graphics were obtained using the ggplot2 v3.3.3, pheatmap v1.0.12 and circlize v0.4.12 packages.

3D representation of known mutations to the RBD surface

Panel D in Figure 5 was prepared with The PyMOL Molecular Graphics System, Version 2.1 Schrödinger, LLC. The atomic model used for the RBD was extracted from the cryo-EM structure of the SARS-CoV-2 spike trimer (PDB:6XR8; Cai et al., 2020)

Affinity measurement using biolayer interferometry (Octet)

This high-throughput kinetic screening of supernatants using single antigen concentration has recently been extensively tested and demonstrated excellent correlation with multiple antigen concentration measurements (Lad et al., 2015). Biolayer interferometry assays were performed using the Octet HTX instrument (ForteBio). Anti-Human Fc Capture (AHC) biosensors (18-5060) were immersed in supernatants from single-cell MBC cultures (or control monoclonal antibody) at 25°C for 1800 seconds. Biosensors were equilibrated for 10 minutes in 10x PBS buffer with surfactant Tween 20 (Xantec B PBST10-500) diluted 1x in sterile water with 0.1% BSA added (PBS-BT) prior to measurement. Association was performed for 600s in PBS-BT with WT or variant RBD at 100nM followed by dissociation for 600s in PBS-BT. Biosensor regeneration was performed by alternating 30s cycles of regeneration buffer (glycine HCl, 10 mM, pH 2.0) and 30s of PBS-BT for 3 cycles. Traces were reference sensor subtracted and curve fitting was performed using a local 1:1 binding model in the HT Data analysis software 11.1 (ForteBio). Sensors with response values (maximum RBD association) below 0.1nm were considered non-binding. WT RBD non-binding monoclonal antibodies (n=14/414) were excluded from further analysis. For variant RBD non-binding mAbs, sensor-associated data (mAb loading and response) were manually checked to ensure that this was not the result of poor mAb loading. Following the final tested RBD variant (B.1.617.2), 18 sensors were excluded due to mAb loading issues, leaving 382 mAb included in the final analysis. For binding clones, only those with full $R^2 > 0.8$ were retained for KD reporting (Figure 4 and Figure S4) and initial prediction of key binding residues. mAbs were defined as affected against a given variant RBD if the ratio of calculated KD value against that RBD variant and the WT RBD was superior to two. Key binding residues prediction was simply made based on mutations repartition in the different variants (**Figure 5C**); for example mAbs affected only by B.1.351 and P.1 variants were predicted to bind to the K417 residue. Two exceptions to these simple rules were made: 1/ mAbs affected by the B.1.1.7, B.1.351 and P.1 variants were initially labeled as binding to the N501 residue but the ratios of KD values against the B.1.351 and P.1 RBD variants and the B.1.1.7 RBD variants were further calculated. All mAbs with ratio superior to two for these two combinations were labeled as binding both the N501 and K417 residues, as previously described for RBS-A type of anti-RBD mAbs (Yuan et al., 2021)); 2/ mAbs affected by the B.1.351, P.1, B.1.617.1 and B.1.617.2 variants, but not the B.1.1.7 variant, were labeled as binding both the E484 and L452 residues based on reported data in the literature for RBS-B/C

antibodies (Yuan et al., 2021; Starr et al., 2021). Sensors with missing values were manually inspected to resolve binding residues attribution, leaving only four with an unresolved profile. This analysis was further confirmed by conserved intra-clonal residue binding as illustrated in **Table S2H**.

Virus neutralization assay

Virus neutralization was evaluated by a focus reduction neutralization test (FRNT). Vero E6 cells were seeded at 2×10^4 cells/well in a 96-well plate 24h before the assay. Two-hundred focus-forming units (ffu) of each virus were pre-incubated with serial dilutions of heat-inactivated sera or B-cell clone supernatants for 1hr at 37°C before infection of cells for 2hrs. The virus/antibody mix was then removed and foci were left to develop in presence of 1.5% methylcellulose for 2 days. Cells were fixed with 4% formaldehyde and foci were revealed using a rabbit anti-SARS-CoV-2 N antibody (gift of Nicolas Escriou) and anti-rabbit secondary HRP-conjugated secondary antibody. Foci were visualized by diaminobenzidine (DAB) staining and counted using an Immunospot S6 Analyser (Cellular Technology Limited CTL). B-cell culture media and supernatants from RBD negative clones were used as negative control. Pre-pandemic serum (March 2012) was used as negative control for sera titration and was obtained from an anonymous donor through the ICAReB platform (BRIF code n°BB-0033-00062) of Institut Pasteur that collects and manages bioresources following ISO (International Organization for Standardization) 9001 and NF S 96-900 quality standards. Percentage of virus neutralization was calculated as $(100 - ((\#foci \text{ sample} / \#foci \text{ control}) * 100))$. Sera IC50 were calculated over 6 four-fold serial dilutions from 1/10 to 1/10000 using the equation $\log(\text{inhibitor})$ vs. normalized response – Variable slope in Prism 9 (GraphPad software LLC). For some of the sera (namely SARS-CoV-2 recovered post-boost), we were not able to obtain a complete neutralization curve and set up an arbitrary IC50 cut off of $>1/2560$ sera dilution. For culture supernatants, two IgG concentrations (80 nM and 16 nM) were tested for each sample and each virus. Potent neutralizers were defined as $>80\%$ neutralization at 16 nM, weak neutralizer as neutralization $<80\%$ at 16 nM but $>80\%$ at 80 nM. Others were defined as non-neutralizing.

Quantification and Statistical Analysis

Ordinary One-way ANOVA, Two-way ANOVA, Repeated measures mixed effects model analysis, Kruskal-Wallis test and Mann-Whitney test were used to compare continuous variables as appropriate (indicated in Figures). Benjamini, Krieger and Yekutieli FDR correction was used for all multiple comparisons. A P -value ≤ 0.05 was considered

statistically significant. Statistical analyses were all performed using GraphPad Prism 9.0 (La Jolla, CA, USA).

Additional resources

ClinicalTrials.gov Identifier: MEMO-CoV2, NCT04402892.

Excel table titles

Table S1. Human subject information. Related to Figures 1, 2, 3, 4, 5 and 6 and Figures S1, S2, S3, S4, S5 and S6.

Table S2. ELISA, neutralization, flow cytometry and affinity data. Related to Figures 1, 2, 4, 5 and 6 and Figures S1, S2, S4, S5 and S6.

Table S3. Single-cell culture and sequencing. Related to Figures 3, 4, 5 and 6 and Figures S3, S4, S5 and S6.

Declaration of interests: Outside of the submitted work, M.M. received research funds from GSK and personal fees from LFB and Amgen; JC.W. received consulting fees from Institut Mérieux; P.B. received consulting fees from Regeneron Pharmaceuticals; JM.P. received personal fees from Abbvie, Gilead, Merck, and Siemens Healthcare; F.R. is a member of the board of MELETIOS Therapeutics and of the Scientific Advisory Board of eureKARE.

Journal Pre-proof

Bibliography.

- Abu-Raddad, L.J., Chemaitelly, H., Butt, A.A., and National Study Group for COVID-19 Vaccination (2021). Effectiveness of the BNT162b2 Covid-19 Vaccine against the B.1.1.7 and B.1.351 Variants. *N Engl J Med* 385, 187–189.
- Andrews, S.F., Huang, Y., Kaur, K., Popova, L.I., Ho, I.Y., Pauli, N.T., Henry Dunand, C.J., Taylor, W.M., Lim, S., Huang, M., et al. (2015). Immune history profoundly affects broadly protective B cell responses to influenza. *Sci Transl Med* 7, 316ra192.
- Baden, L.R., El Sahly, H.M., Essink, B., Kotloff, K., Frey, S., Novak, R., Diemert, D., Spector, S.A., Rouphael, N., Creech, C.B., et al. (2021). Efficacy and Safety of the mRNA-1273 SARS-CoV-2 Vaccine. *N Engl J Med* 384, 403–416.
- Barnes, C.O., West, A.P., Huey-Tubman, K.E., Hoffmann, M.A.G., Sharaf, N.G., Hoffman, P.R., Koranda, N., Gristick, H.B., Gaebler, C., Muecksch, F., et al. (2020). Structures of Human Antibodies Bound to SARS-CoV-2 Spike Reveal Common Epitopes and Recurrent Features of Antibodies. *Cell* 182, 828-842.e16.
- Cai, Y., Zhang, J., Xiao, T., Peng, H., Sterling, S. M., Walsh, R. M., Rawson, S., Rits-Volloch, S., and Chen, B., (2020). Distinct conformational states of SARS-CoV-2 spike protein. *Science* 369, 1586-1592.
- Cele, S., Gazy, I., Jackson, L., Hwa, S.-H., Tegally, H., Lustig, G., Giandhari, J., Pillay, S., Wilkinson, E., Naidoo, Y., et al. (2021). Escape of SARS-CoV-2 501Y.V2 from neutralization by convalescent plasma. *Nature* 593, 142–146.
- Cherian, S., Potdar, V., Jadhav, S., Yadav, P., Gupta, N., Das, M., Das, S., Agarwal, A., Singh, S., Abraham, P., et al. (2021). Convergent evolution of SARS-CoV-2 spike mutations, L452R, E484Q and P681R, in the second wave of COVID-19 in Maharashtra, India. *BioRxiv*. <https://doi.org/10.1101/2021.04.22.440932>
- Cho, A., Muecksch, F., Schaefer-Babajew, D., Wang, Z., Finkin, S., Gaebler, C., Ramos, V., Cipolla, M., Agudelo, M., Bednarski, E., et al. (2021). Antibody Evolution after SARS-CoV-2 mRNA Vaccination. *BioRxiv*. <https://doi.org/10.1101/2021.07.29.454333>
- Crickx, E., Chappert, P., Sokal, A., Weller, S., Azzaoui, I., Vandenberghe, A., Bonnard, G., Rossi, G., Fadeev, T., Storck, S., et al. (2021b). Rituximab-resistant splenic memory B cells and newly engaged naive B cells fuel relapses in patients with immune thrombocytopenia. *Sci Transl Med* 13, eabc3961.
- Dagan, N., Barda, N., Kepten, E., Miron, O., Perchik, S., Katz, M.A., Hernán, M.A., Lipsitch, M., Reis, B., and Balicer, R.D. (2021). BNT162b2 mRNA Covid-19 Vaccine in a Nationwide Mass Vaccination Setting. *N Engl J Med* 384, 1412–1423.
- Davies, N.G., Abbott, S., Barnard, R.C., Jarvis, C.I., Kucharski, A.J., Munday, J.D., Pearson, C.A.B., Russell, T.W., Tully, D.C., Washburne, A.D., et al. (2021). Estimated transmissibility and impact of SARS-CoV-2 lineage B.1.1.7 in England. *Science* 372. eabg3055.
- Dugan, H.L., Stamper, C.T., Li, L., Changrob, S., Asby, N.W., Halfmann, P.J., Zheng, N.-Y., Huang, M., Shaw, D.G., Cobb, M.S., et al. (2021). Profiling B cell immunodominance after

SARS-CoV-2 infection reveals antibody evolution to non-neutralizing viral targets. *Immunity* 54, 1290-1303.e7.

Ebinger, J.E., Fert-Bober, J., Printsev, I., Wu, M., Sun, N., Prostko, J.C., Frias, E.C., Stewart, J.L., Van Eyk, J.E., Braun, J.G., et al. (2021). Antibody responses to the BNT162b2 mRNA vaccine in individuals previously infected with SARS-CoV-2. *Nat. Med.* 27, 981–984.

Edara, V.V., Norwood, C., Floyd, K., Lai, L., Davis-Gardner, M.E., Hudson, W.H., Mantus, G., Nyhoff, L.E., Adelman, M.W., Fineman, R., et al. (2021). Infection- and vaccine-induced antibody binding and neutralization of the B.1.351 SARS-CoV-2 variant. *Cell Host Microbe* 29, 516-521.e3.

Gaebler, C., Wang, Z., Lorenzi, J.C.C., Muecksch, F., Finkin, S., Tokuyama, M., Cho, A., Jankovic, M., Schaefer-Babajew, D., Oliveira, T.Y., et al. (2021). Evolution of antibody immunity to SARS-CoV-2. *Nature* 591, 639–644.

Garcia-Beltran, W.F., Lam, E.C., St. Denis, K., Nitido, A.D., Garcia, Z.H., Hauser, B.M., Feldman, J., Pavlovic, M.N., Gregory, D.J., Poznansky, M.C., et al. (2021). Multiple SARS-CoV-2 variants escape neutralization by vaccine-induced humoral immunity. *Cell* 184, 2372-2383.e9.

Goel, R.R., Apostolidis, S.A., Painter, M.M., Mathew, D., Pattekar, A., Kuthuru, O., Gouma, S., Hicks, P., Meng, W., Rosenfeld, A.M., et al. (2021). Distinct antibody and memory B cell responses in SARS-CoV-2 naïve and recovered individuals following mRNA vaccination. *Sci Immunol* 6. eabi6950.

Greaney, A.J., Loes, A.N., Crawford, K.H.D., Starr, T.N., Malone, K.D., Chu, H.Y., and Bloom, J.D. (2021a). Comprehensive mapping of mutations in the SARS-CoV-2 receptor-binding domain that affect recognition by polyclonal human plasma antibodies. *Cell Host Microbe* 29, 463-476.e6.

Greaney, A.J., Starr, T.N., Barnes, C.O., Weisblum, Y., Schmidt, F., Caskey, M., Gaebler, C., Cho, A., Agudelo, M., Finkin, S., et al. (2021b). Mapping mutations to the SARS-CoV-2 RBD that escape binding by different classes of antibodies. *Nat Commun* 12, 4196.

Gupta, N.T., Vander Heiden, J.A., Uduman, M., Gadala-Maria, D., Yaari, G., and Kleinstein, S.H. (2015). Change-O: a toolkit for analyzing large-scale B cell immunoglobulin repertoire sequencing data. *Bioinformatics* 31, 3356–3358.

Hacisuleyman, E., Hale, C., Saito, Y., Blachere, N.E., Bergh, M., Conlon, E.G., Schaefer-Babajew, D.J., DaSilva, J., Muecksch, F., Gaebler, C., et al. (2021). Vaccine Breakthrough Infections with SARS-CoV-2 Variants. *N Engl J Med.* 384, 2212–2218.

Harvey, W.T., Carabelli, A.M., Jackson, B., Gupta, R.K., Thomson, E.C., Harrison, E.M., Ludden, C., Reeve, R., Rambaut, A., Peacock, S.J., et al. (2021). SARS-CoV-2 variants, spike mutations and immune escape. *Nat. Rev. Microbiol.* 19, 409–424

Hoffmann, M., Arora, P., Groß, R., Seidel, A., Hörnich, B.F., Hahn, A.S., Krüger, N., Graichen, L., Hofmann-Winkler, H., Kempf, A., et al. (2021). SARS-CoV-2 variants B.1.351 and P.1 escape from neutralizing antibodies. *Cell* 184, 2384-2393.e12.

- Hsieh, C.-L., Goldsmith, J.A., Schaub, J.M., DiVenere, A.M., Kuo, H.-C., Javanmardi, K., Le, K.C., Wrapp, D., Lee, A.G., Liu, Y., et al. (2020). Structure-based design of prefusion-stabilized SARS-CoV-2 spikes. *Science* 369, 1501–1505.
- Ju, B., Zhang, Q., Ge, J., Wang, R., Sun, J., Ge, X., Yu, J., Shan, S., Zhou, B., Song, S., et al. (2020). Human neutralizing antibodies elicited by SARS-CoV-2 infection. *Nature* 584, 115–119.
- Konstantinidis, T.G., Zisaki, S., Mitroulis, I., Konstantinidou, E., Kontekaki, E.G., Romanidou, G., Karvelas, A., Nanousi, I., Lazidis, L., Cassimos, D., et al. (2021b). Levels of Produced Antibodies after Vaccination with mRNA Vaccine; Effect of Previous Infection with SARS-CoV-2. *J Clin Med* 10, 2842.
- Krammer, F., Srivastava, K., Alshammary, H., Amoako, A.A., Awawda, M.H., Beach, K.F., Bermúdez-González, M.C., Bielak, D.A., Carreño, J.M., Chernet, R.L., et al. (2021b). Antibody Responses in Seropositive Persons after a Single Dose of SARS-CoV-2 mRNA Vaccine. *N Engl J Med* 384, 1372–1374.
- Lad, L., Clancy, S., Kovalenko, M., Liu, C., Hui, T., Smith, V., and Pagratis, N. (2015). High-throughput kinetic screening of hybridomas to identify high-affinity antibodies using bio-layer interferometry. *J Biomol Screen* 20, 498–507.
- Luo, X.M., Maarschalk, E., O’Connell, R.M., Wang, P., Yang, L., and Baltimore, D. (2009). Engineering human hematopoietic stem/progenitor cells to produce a broadly neutralizing anti-HIV antibody after in vitro maturation to human B lymphocytes. *Blood* 113, 1422–1431.
- Manisty, C., Otter, A.D., Treibel, T.A., McKnight, Á., Altmann, D.M., Brooks, T., Noursadeghi, M., Boyton, R.J., Semper, A., and Moon, J.C. (2021). Antibody response to first BNT162b2 dose in previously SARS-CoV-2-infected individuals. *Lancet* 397, 1057–1058.
- McCallum, M., De Marco, A., Lempp, F.A., Tortorici, M.A., Pinto, D., Walls, A.C., Beltramello, M., Chen, A., Liu, Z., Zatta, F., et al. (2021). N-terminal domain antigenic mapping reveals a site of vulnerability for SARS-CoV-2. *Cell* 184, 2332-2347.e16.
- Mesin, L., Schiepers, A., Ersching, J., Barbulescu, A., Cavazzoni, C.B., Angelini, A., Okada, T., Kurosaki, T., and Victora, G.D. (2020). Restricted Clonality and Limited Germinal Center Reentry Characterize Memory B Cell Reactivation by Boosting. *Cell* 180, 92-106.e11.
- Muecksch, F., Weisblum, Y., Barnes, C.O., Schmidt, F., Schaefer-Babajew, D., Lorenzi, J.C.C., Flyak, A.I., DeLaitch, A.T., Huey-Tubman, K.E., Hou, S., et al. (2021). Development of potency, breadth and resilience to viral escape mutations in SARS-CoV-2 neutralizing antibodies. *Immunity* 54, 1853-1868.e7.
- Planas, D., Bruel, T., Grzelak, L., Guivel-Benhassine, F., Staropoli, I., Porrot, F., Planchais, C., Buchrieser, J., Rajah, M.M., Bishop, E., et al. (2021a). Sensitivity of infectious SARS-CoV-2 B.1.1.7 and B.1.351 variants to neutralizing antibodies. *Nat Med* 27, 917–924.
- Planas, D., Veyer, D., Baidaliuk, A., Staropoli, I., Guivel-Benhassine, F., Rajah, M.M., Planchais, C., Porrot, F., Robillard, N., Puech, J., et al. (2021b). Reduced sensitivity of SARS-CoV-2 variant Delta to antibody neutralization. *Nature* 596, 276–280.

- Plante, J.A., Liu, Y., Liu, J., Xia, H., Johnson, B.A., Lokugamage, K.G., Zhang, X., Muruato, A.E., Zou, J., Fontes-Garfias, C.R., et al. (2021). Spike mutation D614G alters SARS-CoV-2 fitness. *Nature* 592, 116–121.
- Polack, F.P., Thomas, S.J., Kitchin, N., Absalon, J., Gurtman, A., Lockhart, S., Perez, J.L., Pérez Marc, G., Moreira, E.D., Zerbini, C., et al. (2020). Safety and Efficacy of the BNT162b2 mRNA Covid-19 Vaccine. *N Engl J Med* 383, 2603–2615.
- Purtha, W.E., Tedder, T.F., Johnson, S., Bhattacharya, D., and Diamond, M.S. (2011). Memory B cells, but not long-lived plasma cells, possess antigen specificities for viral escape mutants. *J. Exp. Med.* 208, 2599–2606.
- Reynolds, C.J., Pade, C., Gibbons, J.M., Butler, D.K., Otter, A.D., Menacho, K., Fontana, M., Smit, A., Sackville-West, J.E., Cutino-Moguel, T., et al. (2021). Prior SARS-CoV-2 infection rescues B and T cell responses to variants after first vaccine dose. *Science* eabh1282.
- Robbiani, D.F., Gaebler, C., Muecksch, F., Lorenzi, J.C.C., Wang, Z., Cho, A., Agudelo, M., Barnes, C.O., Gazumyan, A., Finkin, S., et al. (2020). Convergent antibody responses to SARS-CoV-2 in convalescent individuals. *Nature* 584, 437–442.
- Rodda, L.B., Netland, J., Shehata, L., Pruner, K.B., Morawski, P.A., Thouvenel, C.D., Takehara, K.K., Eggenberger, J., Hemann, E.A., Waterman, H.R., et al. (2021). Functional SARS-CoV-2-Specific Immune Memory Persists after Mild COVID-19. *Cell* 184, 169-183.e17.
- Saadat, S., Rikhtegaran Tehrani, Z., Logue, J., Newman, M., Frieman, M.B., Harris, A.D., and Sajadi, M.M. (2021). Binding and Neutralization Antibody Titers After a Single Vaccine Dose in Health Care Workers Previously Infected With SARS-CoV-2. *JAMA* 325, 1467–1469.
- Sakharkar, M., Rappazzo, C.G., Wieland-Alter, W.F., Hsieh, C.-L., Wrapp, D., Esterman, E.S., Kaku, C.I., Wec, A.Z., Geoghegan, J.C., McLellan, J.S., et al. (2021). Prolonged evolution of the human B cell response to SARS-CoV-2 infection. *Sci Immunol* 6. eabg6916.
- Samanovic, M.I., Cornelius, A.R., Wilson, J.P., Karmacharya, T., Gray-Gaillard, S.L., Allen, J.R., Hyman, S.W., Moritz, G., Ali, M., Koralov, S.B., et al. (2021). Poor antigen-specific responses to the second BNT162b2 mRNA vaccine dose in SARS-CoV-2-experienced individuals. *MedRxiv*. <https://doi.org/10.1101/2021.02.07.21251311>
- Scheid, J.F., Barnes, C.O., Eraslan, B., Hudak, A., Keefe, J.R., Cosimi, L.A., Brown, E.M., Muecksch, F., Weisblum, Y., Zhang, S., et al. (2021). B cell genomics behind cross-neutralization of SARS-CoV-2 variants and SARS-CoV. *Cell* 184, 3205-3221.e24.
- Sokal, A., Chappert, P., Barba-Spaeth, G., Roeser, A., Fourati, S., Azzaoui, I., Vandenberghe, A., Fernandez, I., Meola, A., Bouvier-Alias, M., et al. (2021). Maturation and persistence of the anti-SARS-CoV-2 memory B cell response. *Cell* 184, 1201-1213.e14.
- Stamatatos, L., Czartoski, J., Wan, Y.-H., Homad, L.J., Rubin, V., Glantz, H., Neradilek, M., Seydoux, E., Jennewein, M.F., MacCamy, A.J., et al. (2021). mRNA vaccination boosts cross-variant neutralizing antibodies elicited by SARS-CoV-2 infection. *Science* eabg9175.

- Starr, T.N., Greaney, A.J., Dingens, A.S., and Bloom, J.D. (2021). Complete map of SARS-CoV-2 RBD mutations that escape the monoclonal antibody LY-CoV555 and its cocktail with LY-CoV016. *Cell Rep Med* 2, 100255.
- Supasa, P., Zhou, D., Dejnirattisai, W., Liu, C., Mentzer, A.J., Ginn, H.M., Zhao, Y., Duyvesteyn, H.M.E., Nutalai, R., Tuekprakhon, A., et al. (2021). Reduced neutralization of SARS-CoV-2 B.1.1.7 variant by convalescent and vaccine sera. *Cell* 184, 2201-2211.e7.
- Tegally, H., Wilkinson, E., Giovanetti, M., Iranzadeh, A., Fonseca, V., Giandhari, J., Doolabh, D., Pillay, S., San, E.J., Msomi, N., et al. (2021). Detection of a SARS-CoV-2 variant of concern in South Africa. *Nature* 592, 438–443.
- Tiller, T., Meffre, E., Yurasov, S., Tsuiji, M., Nussenzweig, M.C., and Wardemann, H. (2008). Efficient generation of monoclonal antibodies from single human B cells by single cell RT-PCR and expression vector cloning. *J. Immunol. Methods* 329, 112–124.
- Turner, J.S., O'Halloran, J.A., Kalaidina, E. et al. (2021). SARS-CoV-2 mRNA vaccines induce persistent human germinal centre responses. *Nature* 596, 109–113.
- Wang, P., Nair, M.S., Liu, L., Iketani, S., Luo, Y., Guo, Y., Wang, M., Yu, J., Zhang, B., Kwong, P.D., et al. (2021a). Antibody resistance of SARS-CoV-2 variants B.1.351 and B.1.1.7. *Nature* 593, 130–135.
- Wang, Z., Muecksch, F., Schaefer-Babajew, D., Finkin, S., Viant, C., Gaebler, C., Hoffmann, H.-H., Barnes, C.O., Cipolla, M., Ramos, V., et al. (2021b). Naturally enhanced neutralizing breadth against SARS-CoV-2 one year after infection. *Nature* 595, 426–431.
- Weisel, F.J., Zuccarino-Catania, G.V., Chikina, M., and Shlomchik, M.J. (2016). A Temporal Switch in the Germinal Center Determines Differential Output of Memory B and Plasma Cells. *Immunity* 44, 116–130.
- Weissman, D., Alameh, M.-G., de Silva, T., Collini, P., Hornsby, H., Brown, R., LaBranche, C.C., Edwards, R.J., Sutherland, L., Santra, S., et al. (2021). D614G Spike Mutation Increases SARS CoV-2 Susceptibility to Neutralization. *Cell Host Microbe* 29, 23-31.e4.
- Woodruff, M.C., Ramonell, R.P., Nguyen, D.C., Cashman, K.S., Saini, A.S., Haddad, N.S., Ley, A.M., Kyu, S., Howell, J.C., Ozturk, T., et al. (2020). Extrafollicular B cell responses correlate with neutralizing antibodies and morbidity in COVID-19. *Nat. Immunol.* s41590-020-00814.
- Xie, X., Liu, Y., Liu, J., Zhang, X., Zou, J., Fontes-Garfias, C.R., Xia, H., Swanson, K.A., Cutler, M., Cooper, D., et al. (2021). Neutralization of SARS-CoV-2 spike 69/70 deletion, E484K and N501Y variants by BNT162b2 vaccine-elicited sera. *Nat Med* 27, 620–621.
- Yuan, M., Huang, D., Lee, C.-C.D., Wu, N.C., Jackson, A.M., Zhu, X., Liu, H., Peng, L., van Gils, M.J., Sanders, R.W., et al. (2021). Structural and functional ramifications of antigenic drift in recent SARS-CoV-2 variants. *Science* 373, 818–823.
- Yurkovetskiy, L., Wang, X., Pascal, K.E., Tomkins-Tinch, C., Nyalile, T.P., Wang, Y., Baum, A., Diehl, W.E., Dauphin, A., Carbone, C., et al. (2020). Structural and Functional Analysis of the D614G SARS-CoV-2 Spike Protein Variant. *Cell* 183, 739-751.e8.

Highlights

1. Vaccination boosts high-affinity RBD-memory B cells (MBCs) in COVID-19 recovered patients
2. Boosted MBCs retain their diversity and express potent variant-neutralizing antibodies
3. SARS-CoV-2-naïve individuals show low serum neutralization of variants after vaccination
4. Maturation of MBCs in naïve individuals allows them to respond to variants of concern

In brief / eTOC blurb

To better understand B cell responses to SARS-CoV-2 mRNA vaccination, Sokal et al. analyzed memory B cells from COVID-19-recovered and -naïve individuals. In recovered patients, vaccination amplifies a broad repertoire of matured MBCs and generates variant-neutralizing plasma cells. In naïve individuals, vaccination induces an MBC pool containing potent neutralizing clones against all current variants of concern, including beta and delta.

Figure 1

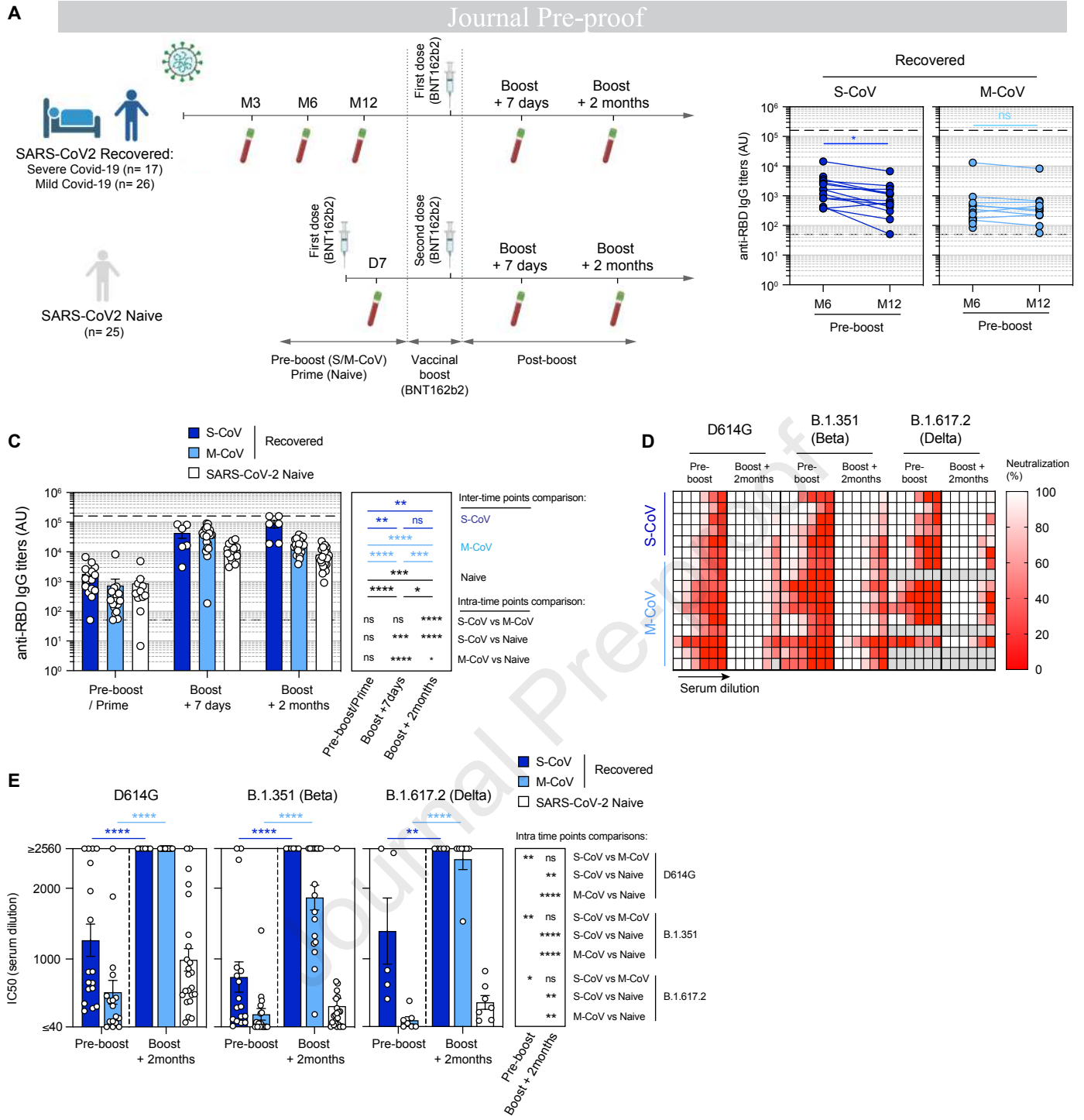


Figure 2

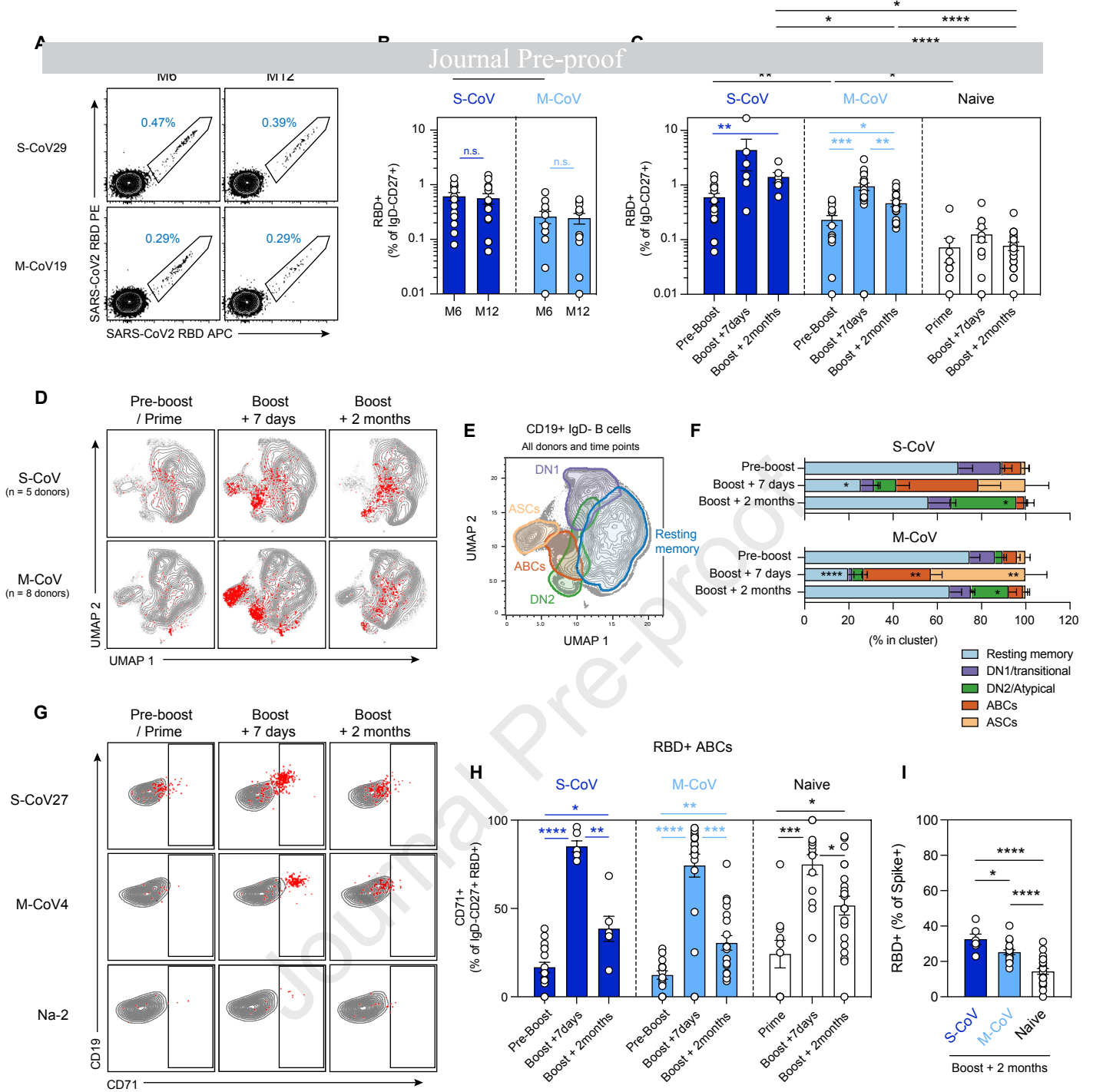


Figure 3

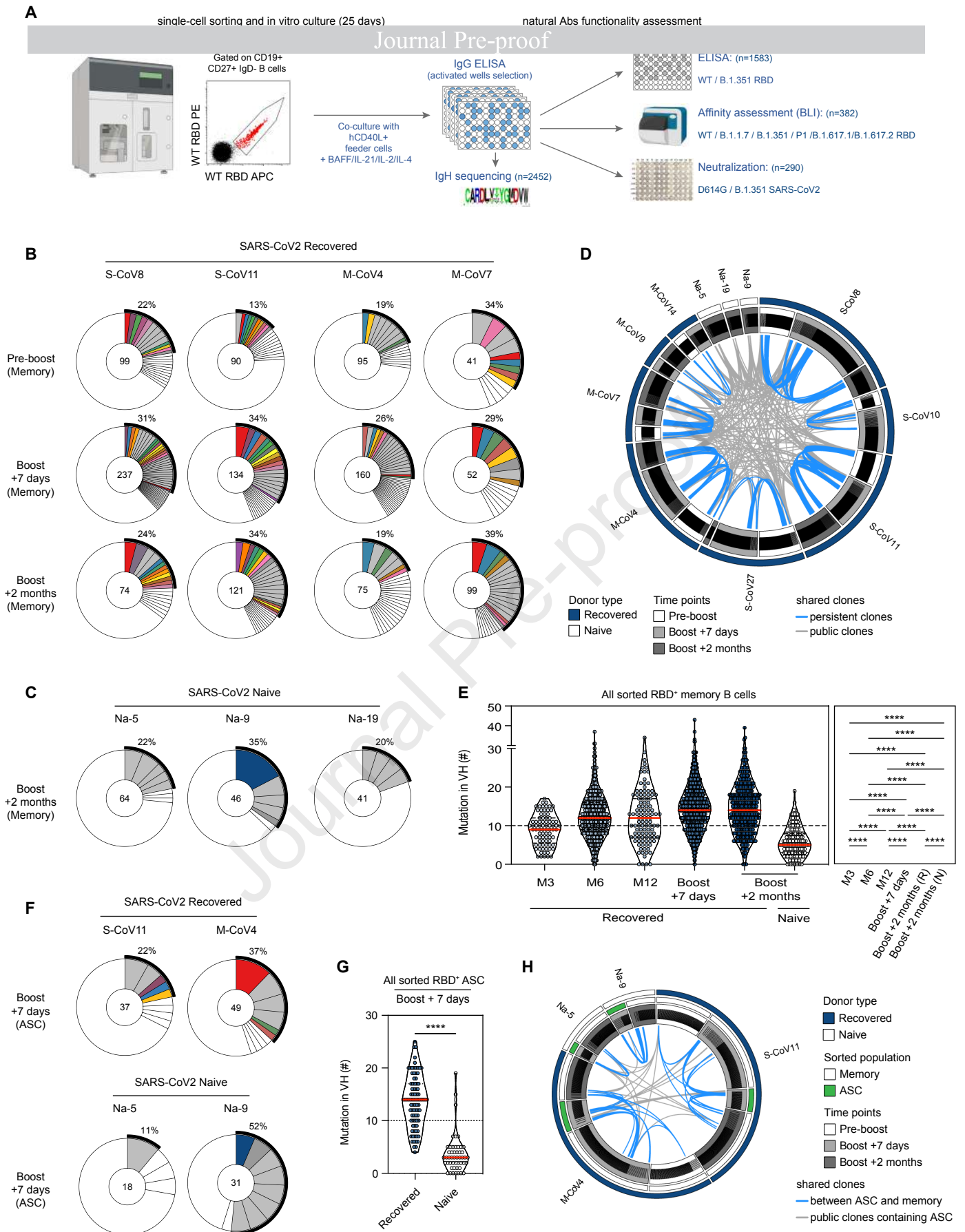


Figure 4

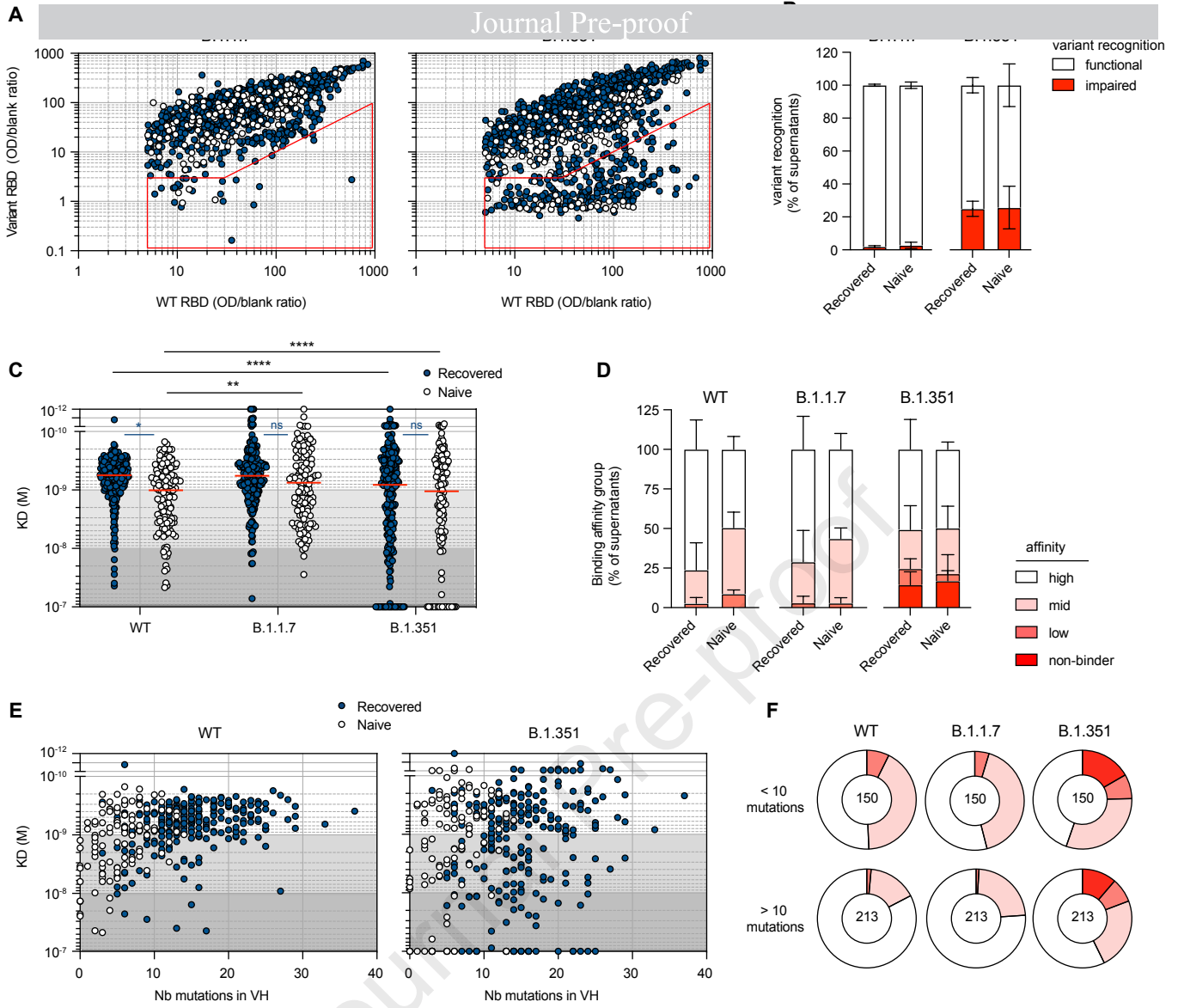


Figure 5

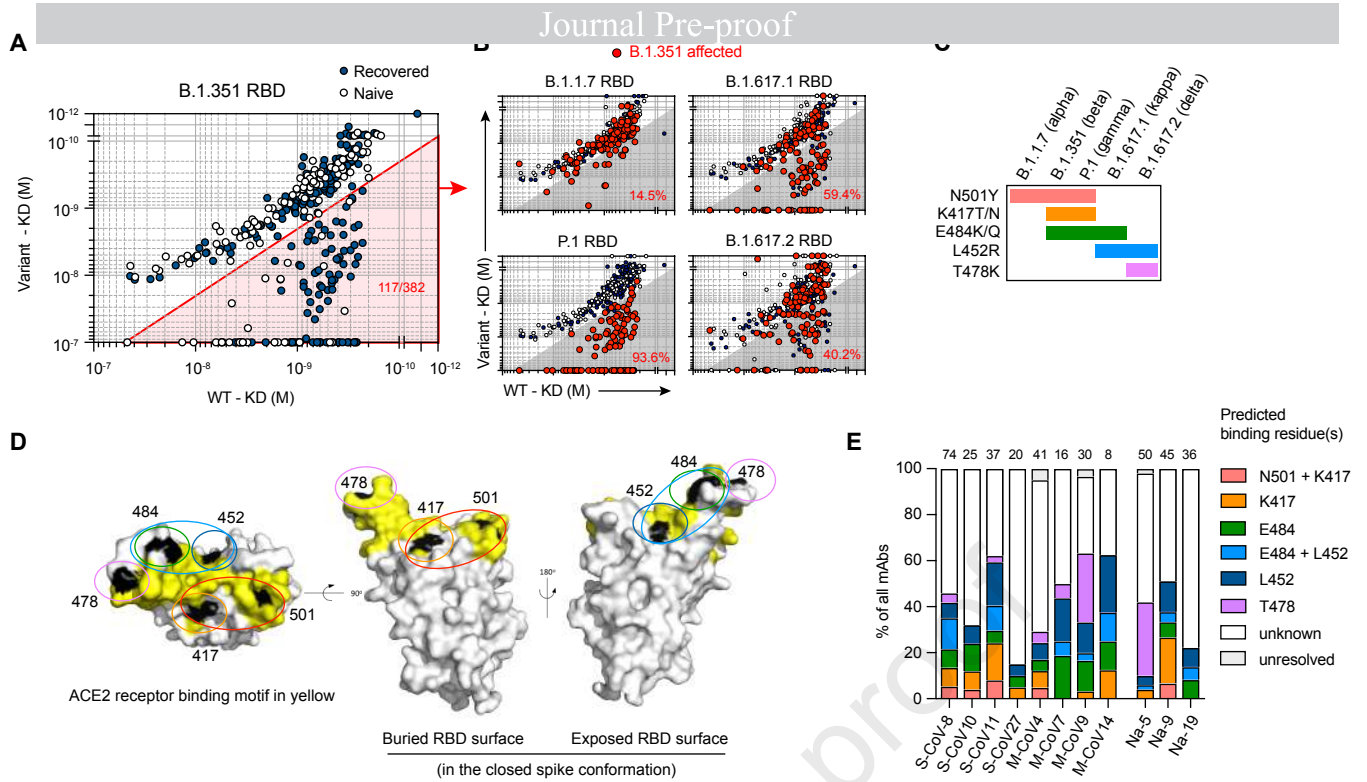


Figure 6

